# Joint Centre for Mesoscale Meteorology, Reading, UK

## Mesoscale aspects of extratropical cyclones: an observational perspective

K. A. Browning

Internal Report No. 44

January 1995

**Met Office** Joint Centre for Mesoscale Meteorology Department of Meteorology
University of Reading PO Box 243 Reading RG6 6BB United Kingdom
Tel: +44 (0)118 931 8425 Fax: +44 (0)118 931 8791
www.metoffice.com

*Designed and produced by the Met Office © Crown copyright 2001 01/0240 The Met Office logo is a registered trademark.*

Version dated January 95

# Mesoscale aspects of extratropical cyclones: an observational perspective

**[Review paper prepared for the Bergen Post-Conference Volume]**

**K A Browning**
**University of Reading, UK**

## 1. Introduction

Our understanding of the mesoscale structure of frontal cyclones has, as we show in this review, benefitted greatly from special mesoscale observations such as dropwindsondes and other measurements from aircraft. These observations are usually interpreted within the context of numerical weather prediction (NWP) model analyses based on the more conventional operational synoptic-scale observations. A few studies have also used high-resolution mesoscale models to assimilate the observations and results from some of these studies are included in this review. Another tool for mesoscale analysis - and a major source of inspiration for this review - is imagery. This includes cloud and water-vapour imagery from satellites, especially geostationary satellites, and also precipitation imagery from ground-based radar, especially in networks. By providing the overall pattern of the mesoscale phenomena and an indication of the relationship to the larger-scale forcing, the imagery is invaluable for providing qualitative understanding of the processes at work. Often it provides the only clues as to what is happening on the mesoscale.

There is a whole range of cyclone structures and evolutions which it is convenient to categorize according to the synoptic-scale setting. To ease the presentational task we shall, however, restrict our scope mainly to one particular class of cyclone. Another limitation in the scope of this review is that we shall tend to focus on cyclones in and near NW Europe. Reference will be made to observational studies in North America and elsewhere but the specific cases illustrated in detail will be drawn from European experience at the eastern end of the North Atlantic storm track. By referring to a self-consistent set of examples, we are able to portray more clearly how all the bits fit together into a coherent picture. Despite this

restrictive approach, we believe that the conceptual framework that we shall present has a broader applicability. The notions of conveyor belts, dry intrusions and frontal fractures which we use to unify the observations, whilst not helpful in every context, do provide a useful framework within which to visualize and interpret 3-dimensional mesoscale organization.

One of the earliest satellite-based cyclone classification schemes was by Zillman and Price (1972), later adapted by Browning and Hill (1985) - see Fig 1. The scheme identifies three types of cyclogenesis according to the distance between the area of enhanced cumulus or comma cloud, associated with an upper-level trough, on one hand, and a pre-existing polar-front cloud band on the other. When the two remain completely separate the cyclogenesis is referred to as a comma cloud type. When the clouds associated with the upper-level trough begin as a separate entity and later merge with the frontal cloud band to give a lambda-shaped cloud system, the process is referred to as instant occlusion. And when the cyclogenesis occurs close to the polar-front cloud band and involves it dynamically from an early stage, it is referred to as a frontal-wave type development: this is the type of cyclone we shall be focusing on in this review.

A recent satellite-based study of rapidly-developing cyclones in the western North Atlantic by Evans et al (1994) has modified the above classification by adding, as a fourth category, a variant of the instant occlusion which they refer to as a 'left exit' type. Otherwise their study confirms the three categories in the earlier scheme. Evans et al, however, rename the 'frontal wave' type as the 'emerging cloud head' type. This is in recognition of a characteristic cloud feature that we shall later be describing in detail (Sec. 3). Emerging-

cloud-head cyclogenesis corresponds to the type of development in the Weldon (1977) scheme in which a so-called baroclinic leaf cloud forms directly over a low-level baroclinic zone.

Within the category of cyclone known as the 'frontal wave' or 'emerging cloud head' type, a variety of different configurations can occur depending on the synoptic-scale upper-air flow pattern. Young (1994) distinguishes between cyclones of this kind that develop in the presence of (a) a meridional trough, (b) a flat trough with confluent flow and (c) a flat trough with diffluent flow. An indication of these sub-types is shown in Fig 2 and the cases we shall be describing in this review are all believed to be related to these sub-types. A problem with detailed classification schemes in nature is that there generally tends to be a continuous spectrum of possibilities; however, we shall be concerned not so much with the differences between these sub-types as with the features that are common to all of them, namely the cloud head (labelled E in Fig 2), the polar-front cloud band (labelled F) and the dry slot that intrudes into the centre of the cyclone and marks the position of a feature known as the dry intrusion (Sec 4).

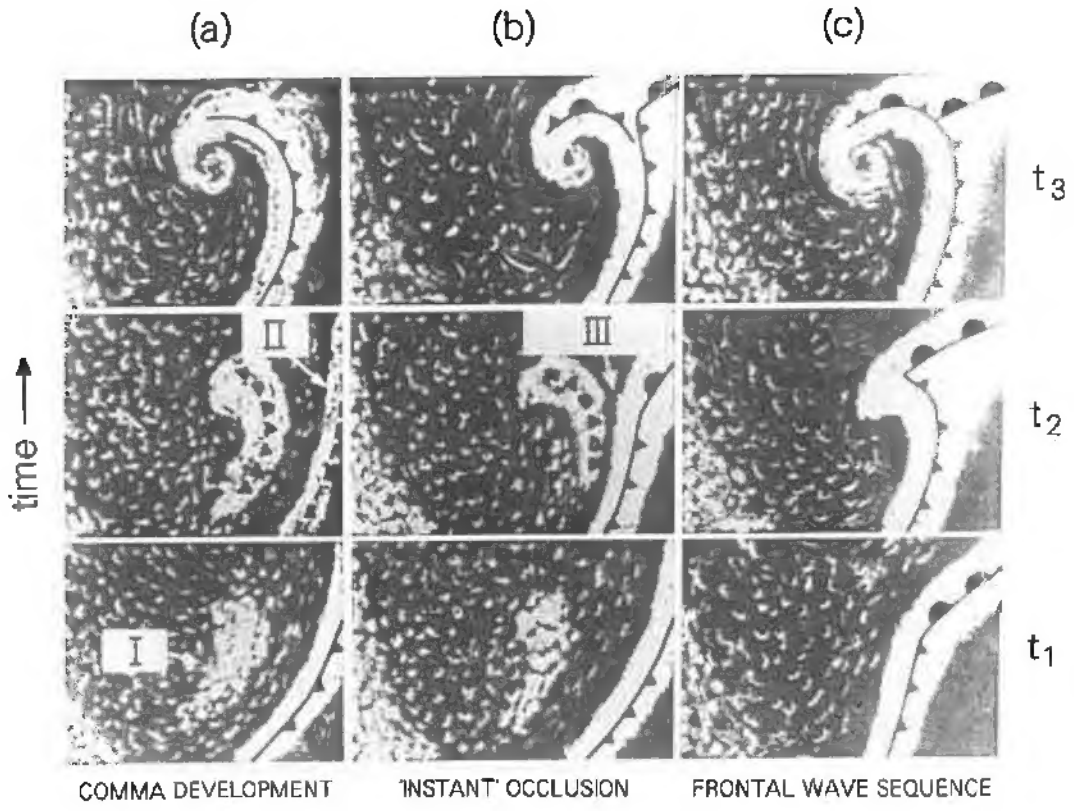


Fig.1 Schematic depiction of three basic sequences of vortex development evident in satellite imagery: (a) development of a simple comma cloud entirely within the cold air, (b) development of an instant occlusion, (c) development of a frontal wave (adapted from Zillman and Price 1972 by Browning and Hill 1985). Frontal symbols represent the original authors' way of representing the various evolution sequences using the tools of conventional frontal analysis. The labels I, II and III, respectively, indicate a region of enhanced convection, a decaying cloud band and a convective cloud band merging with the polar-front cloud band.

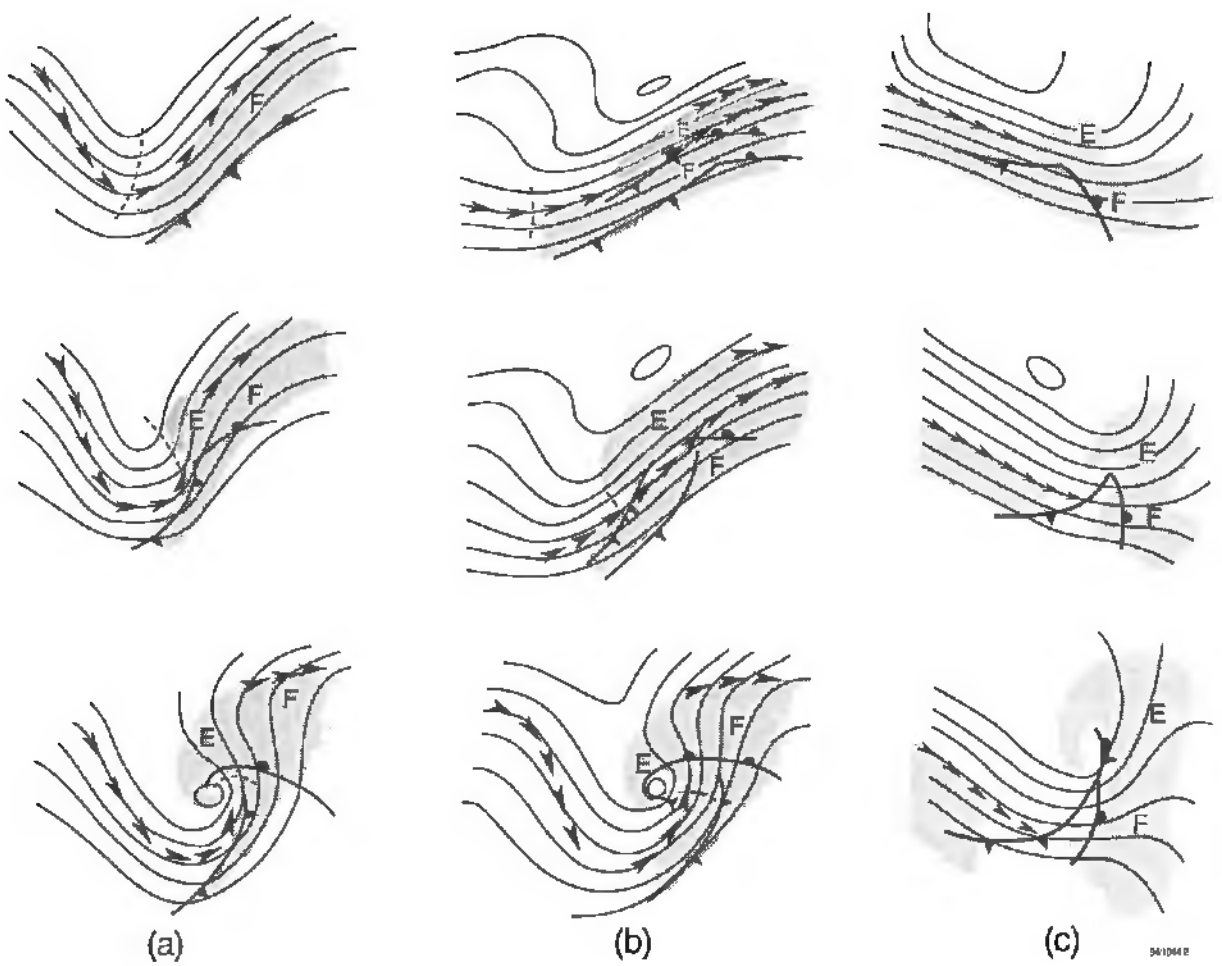


Fig.2 Idealised life-cycles of extratropical cyclones developing in three types of upper flow pattern: (a) meridional trough, (b) flat-trough confluent flow and (c) flat-trough diffluent flow. Continuous lines are idealised contours of 300 mb height. Bold arrows represent jet axes. Stippling represents areas of significant middle and upper cloud. F is cloud associated with the main frontal zone whilst E represents new layered cloud forming during cyclogenesis. Where darker shading is used for E, it represents predominantly middle-level cloud. The dashed line indicates a mobile short-wave trough. (Young 1994).

## 2. Conceptual framework

### 2.1 Frontal fracture

A conceptual model that provides a useful framework for the kind of cyclones discussed in this review is the life-cycle model of Shapiro and Keyser (1990) (Fig 3), aspects of which were anticipated by McGinnigle et al (1988). The first stage in this life cycle shows the incipient frontal cyclone. The second and third stages show the development of the so-called frontal fracture in which the main cold front to the south of the cyclone centre advances ahead of the centre whilst cold air to the north of the warm front travels rearwards and wraps around the cyclone centre. The boundary of the latter flow goes close to the low centre to give what traditional synopticians refer to as a bent-back occlusion. McGinnigle et al (1988) and Shapiro and Keyser (1990) reanalyse the bent-back occlusion as a bent-back warm front, although part of it does in fact advance with a component towards the warm air and is properly analysed as a cold front. We shall refer to it simply as the bent-back front. Meanwhile, as the bent-back front develops, the temperature gradient in the northern part of the original cold front weakens and air from the warm sector in this region gets drawn towards the low centre. As the cyclone matures the bent-back front begins to encircle the low centre and tends to seclude a core of warm air at the centre.

The true surface cold front may advance several hundred kilometres ahead of the cyclone centre. But often, as in some of the examples illustrated in this review, it advances only 200-300km ahead of the cyclone centre. Given good radar network data, the frontal fracture is perhaps most easily observed in the pattern of precipitation; Fig 4 shows a typical

pattern as seen at Stage 2 of frontal fracture. Polewards of the bent-back front and warm front there is a broad area of widespread precipitation associated with the cloud-head feature discussed in Sec 3. Along the main cold front there is a narrower band of rain which becomes patchy at its northern end where the surface temperature gradient weakens.

In some cases during frontal fracture the true warm-sector air approaching the cyclone centre may be detected only some distance above the surface (eg Kuo et al 1992). In other cases the warm-sector air may remain detectable at the surface all the way to the cyclone centre and bent-back front as in Fig 5 - see bold arrow. (The small decrease in wet-bulb potential temperature ($\theta_w$) along the axis of the bold arrow may be attributable to mixing down of air with lower $\theta_w$ from the overrunning dry intrusion - see later). The analysis in Fig 5 shows the surface cold front terminating 300km short of the warm front. The surface $\theta_w$-gradient associated with this cold front is continuous with that associated with the southwestern end of the bent-back front but the gradient is weak in the gap (dislocation) between the two analysed fronts. The precipitation pattern associated with Fig 5 (not shown) was very similar to that in Fig 4: thus, for example, the belt of rain associated with the main cold front extended as patchy rain beyond the northern end of the surface cold front. Such rain is due to an upper-level front which marks the leading edge of dry air aloft. This upper front, to a first approximation, is often continuous with the main surface cold front, as in Fig 4. Between this upper-level front and the bent-back front, the capping of the warm moist low-level air by dry air tends to inhibit precipitation just to the warm side of the cyclone centre. To understand these features we need to visualise the 3-dimensional thermodynamic structure and the airflows that give rise to it. A way of doing this is to use the concepts of conveyor belts and the dry intrusion.

## 2.2 The principal airstreams

The notion of air masses was enshrined in the early Norwegian models of frontal cyclones. To visualise the detailed 3-dimensional structure of cyclones we find it helpful to extend the air-mass concept by focusing on more or less distinct airstreams known as conveyor belts. These are defined in a frame of reference moving with the cloud systems they produce. Relative-flow analyses within surfaces of constant wet-bulb potential temperature ($\theta_w$) enable one to build up an overall picture of these cloud-generating conveyor-belt flows which can then be related to the available imagery.

The first use of this terminology was by Harrold (1973) since when the term warm conveyor belt (WCB) has been used to describe the flow of air with high $\theta_w$ in frontal systems. Ahead of a cold front there is often a strong and more-or-less well-defined tongue of high-$\theta_w$ airflow that justifies the name conveyor belt in the sense that the air is conveyed with a strong component along its axis. However, when a frontal wave develops, the wave travels along the front so that, relative to the wave, the flow within the conveyor belt is slower and less like a conveyor belt. As the cyclone develops, the isentropic surfaces become increasingly distorted with time and it becomes difficult to carry out relative-flow analyses. Thus it has been argued by Kuo et al (1992) that the concept is no longer useful in the region of developing cyclones. These difficulties are real but, so long as its limitations are kept in mind, the conveyor-belt paradigm still provides a helpful device for qualitatively visualizing 3-dimensional cyclone structure and in particular for providing a framework for interpreting mesoscale structure. Indeed, as we now show, the conveyor-belt concept has been extended beyond that originally envisaged by Harrold.

Fig 6 (a,b,c) shows the conveyor-belt portrayal of cyclone structure in the framework of frontal fracture and Fig 6 (d,e,f) shows three actual radiosonde ascents to illustrate the vertical structure implied by the conveyor belt analysis. The stage of cyclone development depicted here corresponds to Stage 2 of Shapiro and Keysers' (1990) model. Three conveyor belts are shown in Fig 6(a) by broad arrows, and it should be kept in mind that each arrow represents the instantaneous motion of air parcels relative to the system, (individual parcels do not have sufficient time to travel along the entire length of each arrow):

- the primary warm conveyor belt, W1 (after Harrold 1973). This is the main belt of high-$\theta_w$ air that rises from the low troposphere to the upper troposphere within the polar-front cloud band. Objective criteria for identifying the warm conveyor belt (WCB) have been developed and evaluated by Wernli and Rossa (1994). The WCB first travels along the main cold front, often accompanied by a 25 m $s^{-1}$ low-level jet, and then it ascends over the warm front as in Bergeron's (1937) model of an ana-warm front. Fig 6(d), depicting a radiosonde ascent in the region just before the WCB rises above the warm front, shows that the WCB is characterised by a deep layer of high-$\theta_w$ air. The WCB should not be regarded as a closed tube of air conveying only air parcels from one end to the other; rather the WCB flow is augmented by warm low-level air entering it along much of its length (Letestu 1994). Depending on the circumstances, a wave or waves may form on the main cold front (not shown in Fig 6), in which case parts of the WCB may undergo rearward-sloping ascent over the cold air as it travels along the cold front.

● the secondary warm conveyor belt, W2 (after Young et al 1987). This flow, of limited length in the configuration shown in Fig 6, is derived from low-level air near the cyclone centre and includes air coming from the lower part of W1 which peels off towards the cyclone centre. This air ascends at the bent-back front into the feature known at the cloud head (see Sec 3). Fig 6(e), depicting a radiosonde ascent just to the north of the bent-back front, shows the layer of high-$\theta_w$ air corresponding to W2, the top of which marks the top of the cloud head. The W2 flow is part of the ageostrophic transverse circulation at the exit of an upper-level jet streak (Young 1989), enhanced by frictional turning within the boundary layer. It is responsible for bringing the low-level flow of high-$\theta_w$ air into the region of frontal fracture (cf Fig 5).

● the cold conveyor belt, CCB (after Carlson 1980). This is an airstream which, relative to the moving cyclone, initially flows rearwards at low levels along the cold side of the warm front and bent-back front. The CCB is often associated with a low-level jet, occasionally exceeding 25 m $s^{-1}$ as for example in the Great Storm of October 1987 (Shutts 1990, Bader et al 1994). Fig 6(f), depicting a radiosonde ascent just to the north of the bent-back front, as in Fig 6(e) but farther along it towards the southwest, again shows the layer of moist high-$\theta_w$ air corresponding to W2, but beneath it the cold airflow is seen to have strengthened to become a well-defined CCB. Some of the air at the outer edge of the CCB descends, especially where precipitation falling from above evaporates and cools it, but most of the CCB air eventually rises and fans out within the cloud head (Sec 3). Whereas W1 and W2

each tend to be characterised by a rather narrow range of $\theta_w$, the CCB may contain a significant range of $\theta_w$-values because it occurs within the warm frontal zone.

A fourth airstream, shown in Fig 6(c), is:

- the dry intrusion (using the terminology of Rodgers et al 1985 and Young et al 1987). This is part of a dry airstream, characterised by low $\theta_w$, that descends from high levels behind the cyclone and approaches the cyclone centre at middle levels to give a so-called dry slot in the satellite imagery. This dry slot is best seen in the infra-red and water vapour channels. In the dry slot the dry-intrusion air begins to ascend over a shallow moist zone (SMZ) characterized by the high-$\theta_w$ air in W2. The leading edge of the dry intrusion, where it overruns the moist air, is marked in Fig 6(b) as an upper cold front (UCF), strictly an upper cold $\theta_w$-front (see Sec. 4.1).

The configuration in Fig 6 is a common one and it forms the basis for much of the discussion in this review. However, as indicated by Fig 2, the airstreams take on different configurations in different synoptic settings. Fig 6 displays aspects of both Young's 'meridional trough' and his 'flat trough confluent flow' sub-types. A distinctly different structure is shown in Fig 7, corresponding to Young's 'diffluent flow' sub-category. Most of the ingredients of Fig 6 are present in Fig 7 but they are reconfigured. The W2 feature, in particular, is more elongated than the W2 flow in Fig 6. As in Fig 6, a dry intrusion overruns part of W2. We return to this overrunning process later (Sec 4.1).

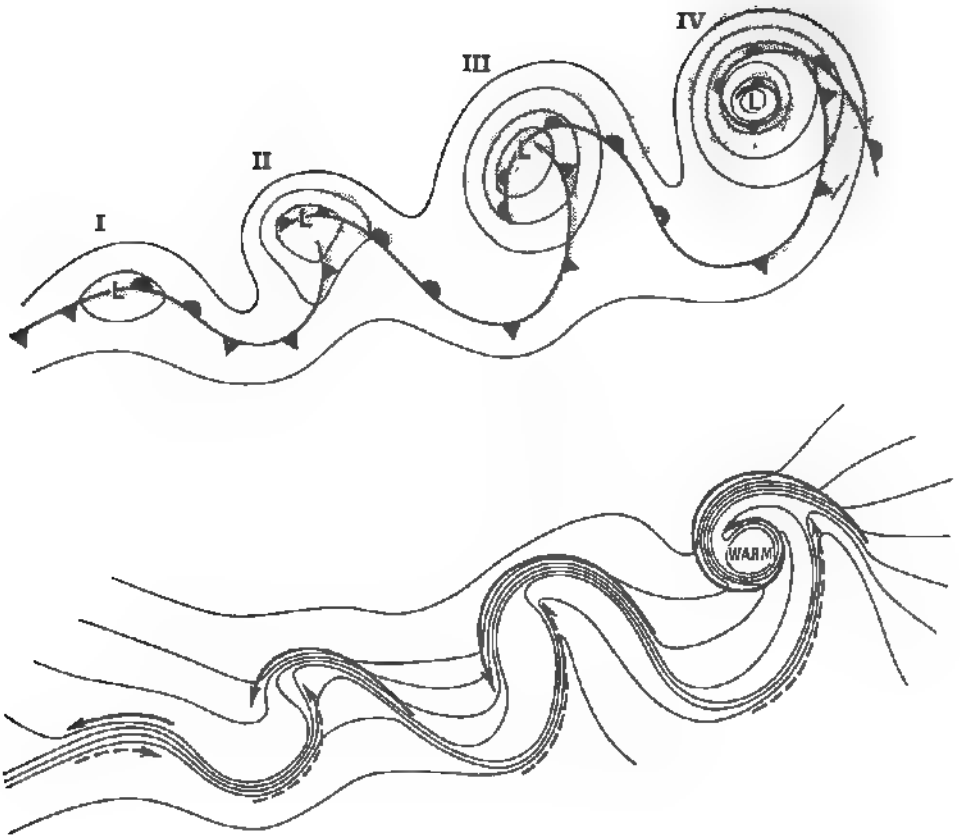


Fig.3 The life cycle of a marine extratropical frontal cyclone (Shapiro and Keyser 1990): (I) incipient frontal cyclone; (II) frontal fracture; (III) bent-back warm front and frontal T-bone; (IV) warm-core frontal seclusion. Upper: sea-level pressure, solid lines; fronts, bold lines; and cloud signature, shaded. Lower: temperature, solid lines; cold and warm air currents, solid and dashed arrows, respectively.

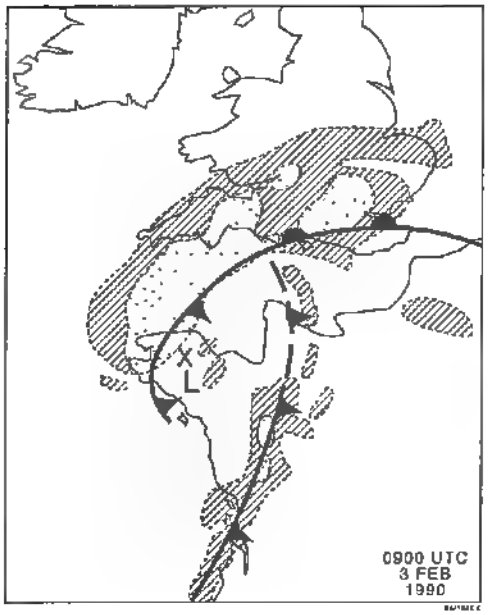


Fig.4 Rainfall distribution and intensity derived from radar data for a cyclone centred over Brittany. Hatching represents rainfall rates less than or equal to 4 mm $h^{-1}$ and stippling greater than 4 mm $h^{-1}$. Surface fronts are shown solid; the dashed front is an upper-level feature. (Young 1994).

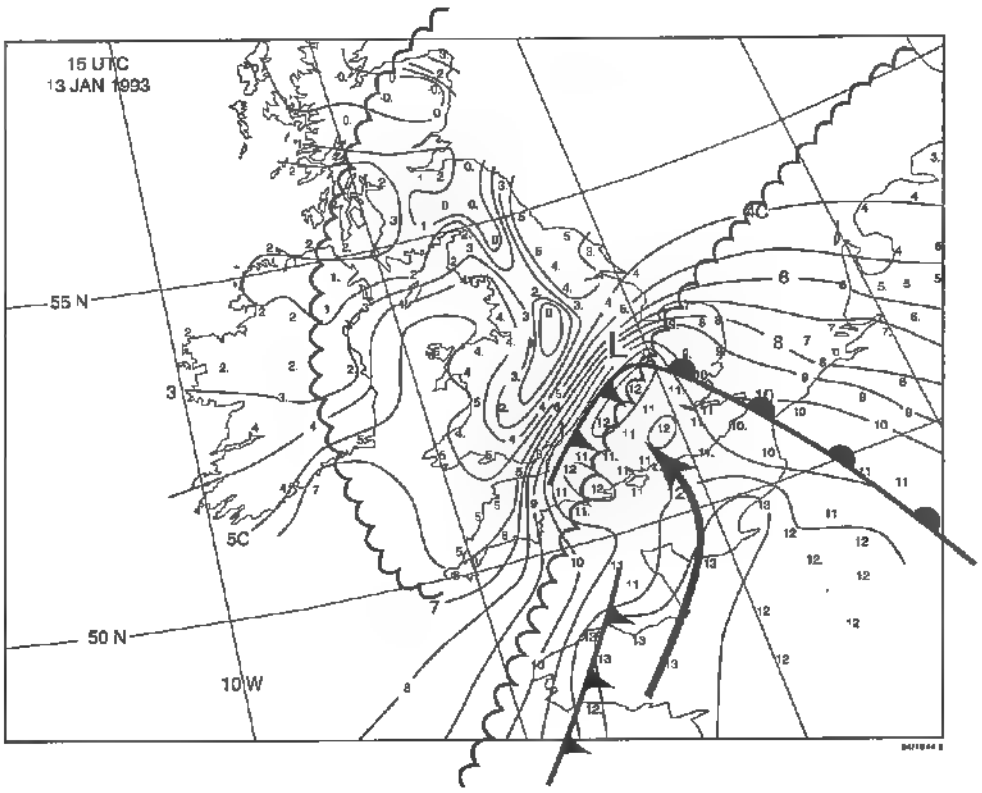


Fig.5 Surface $\theta_w$ and frontal analysis for a cyclone over central England. Individual station values of wet-bulb temperature adjusted to 1000 mb, are plotted to the nearest ½ deg C (½ is indicated by •) and the corresponding isopleths are drawn at 1 deg C intervals. The bold arrow is referred to in the text (Browning and Roberts 1994).

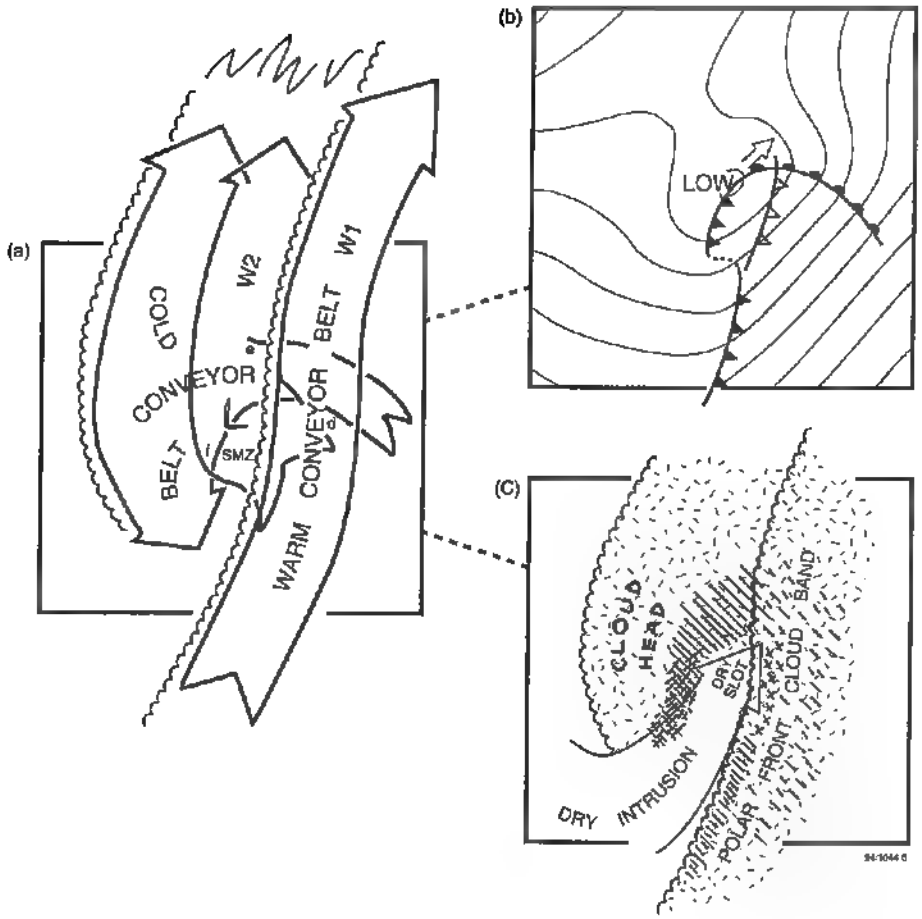


Fig.6(a,b,c) Airflow and precipitation within a developing extratropical frontal cyclone (based on Browning and Roberts 1994).

(a) Conveyor belt analysis. System-relative motion for the three key moist flows:

- Main warm conveyor belt (WCB) labelled W1.
- Cold conveyor belt (CCB) whose ascending diffluent flow is responsible for a large proportion of the cloud head (see (c)).
- Lower part of WCB which peels off and ascends as flow W2 in the top part of the cloud head. The westward component of flow within W2 and the CCB is associated with the ageostrophic transverse circulation at the exit of an upper-level jet streak.

(b) Sea-level pressure (4mb intervals) and frontal analysis. The low is travelling towards the top right. Surface warm front is shown conventionally. Part of the bent-back front is shown as a cold front. The rest of the cold front is shown with closely spaced frontal symbols where it is sharp. The open cold frontal symbols show where it is detectable only aloft (UCF). In between the two sharp surface cold fronts there is a diffuse surface cold frontal zone represented by a dashed line.

(c) Cloud and surface precipitation analysis. Regions of cloud without surface precipitation are shown stippled. The western boundaries of two major cloud features are drawn scalloped: the cloud feature occupying the left half of the diagram is the cloud head; the cloud occupying the right half is the main polar-front cloud band associated with the warm conveyor belt (see W1 in (a)). Cloud- head precipitation, moderately heavy in places, is shown by solid hatching (cross-hatched where convective). A band of heavy rain along the main surface cold front is also shown by solid hatching. Broken hatching represents warm-conveyor-belt rain. Broken cross-hatching represents patchy moderate rain associated with the upper cold front. The arrow labelled 'dry intrusion' shows the system-relative motion of the dry air that descends from near the tropopause upwind and reascends while approaching the cyclone centre where it overruns a shallow moist zone associated with W2 (see SMZ in (a)).

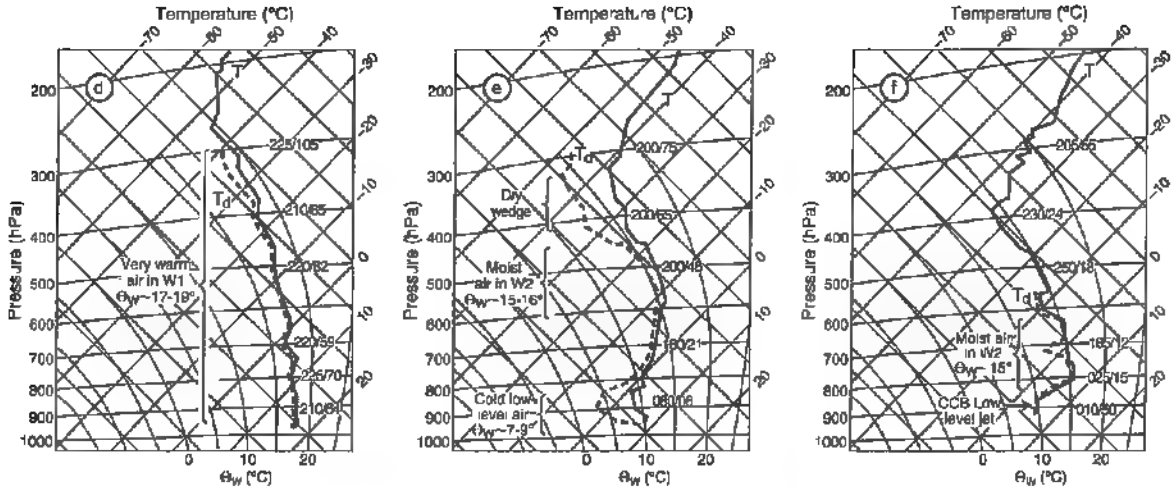


Fig.6 (d,e,f) Actual radiosonde soundings obtained at locations corresponding to d, e and f in Fig.6(a). Temperature and dew point are shown as solid and dashed curves, respectively, and winds are in degrees and knots. The feature labelled 'dry wedge' in (e) is the leading edge of the dry intrusion air where it is lifted above the cloud head. (From Bader et al. 1994).

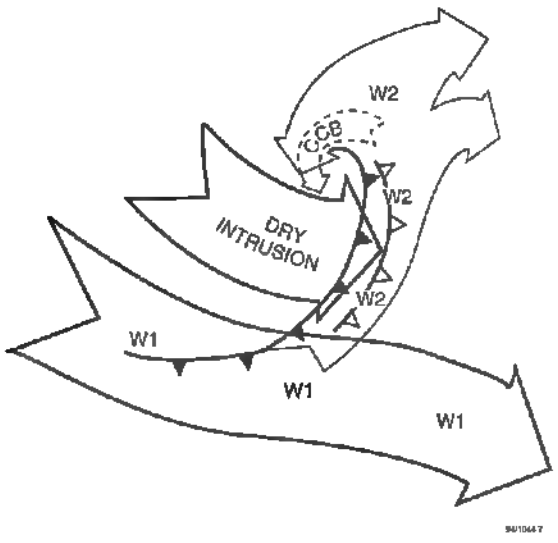


Fig.7 Conceptual model showing system-relative airflows within a cyclone forming ahead of a strongly diffluent trough. The arrows labelled W1 and W2 are warm conveyor belts. The dashed arrow labelled CCB is a shallow cold conveyor belt which forms a hook of low cloud around the cyclone centre. (After Young 1994).

## 3. The cloud head

The occurrence in cyclones of a feature called a cloud head has been alluded to above. The term was coined by Böttger et al (1975) to describe an entire cloud system the northern edge of which develops a sharp convex-poleward boundary during cyclogenesis. We adopt a more restrictive definition (see Fig 6(c)) that confines use of the term to the portion of cloud associated with the bent-back front, whose tops rise from south to the north. This cloud is often a well-defined entity, commonly separated from the polar-front cloud band by a dry slot. A cloud head often takes on a hook shape during cyclogenesis; Young (1994) refers to this as the cloud hook, but we shall retain the term cloud head to describe the feature both before and after it develops a hook shape. Bader et al (1994) restrict the use of the term 'cloud head' to situations preceding rapid cyclogenesis; however, we shall adopt a broader usage embracing situations during rapid deepening and when a similar cloud pattern accompanies a more modest rate of deepening, provided the cloud-head feature is distinct from the polar-front cloud band.

The cloud head is such a characteristic feature that, as mentioned earlier, Evans et al (1994) in their classificaiton scheme were led to refer to frontal wave cyclones as emerging-cloud-head cyclones, ie cloud head emerging from beneath the polar-front cloud band. Not all cloud heads 'emerge', however; sometimes they form alongside (poleward) of the polar-front cloud band (see Fig 2(b) compared with Fig 2(a)). When a cloud head does emerge from beneath a polar-front cloud band during the course of cyclone development, it does so in the manner shown by the satellite image sequence in Fig 8. The whiteness of the cloud pattern in this figure is a measure of the height (coldness) of the cloud top and the grey cloud

head can be seen emerging in the 03UT/13 Jan image on the left side, just west of the low centre, labelled X. The cloud head grows with time during the rapid deepening of the cyclone and at the end of this sequence can be seen to be developing into a major hook-shaped feature.

Coloured lines superimposed on the cloud images in Fig 8 represent the ascending portions of the warm-conveyor-belt W1 (red) and cold-conveyor-belt (blue) flows drawn relative to the moving system. (For simplicity the W2 flow is not depicted in Fig 8 but it is shown in the more detailed portrayal of the same cloud head in Fig 9). Initially in Fig 8 there is no cloud head: the red flow predominates and is responsible for the leaf cloud that develops into a sharp-edged feature from an initially ragged area of deep cloud. The red flow originates as a belt of strong winds with high $\theta_w$ situated at low levels on the equatorward side of the front. It ascends slantwise within the cloud shield north of the front producing substantial precipitation in this region. Although the flow relative to the earth is orientated nearly parallel to the front, its orientation takes on the more northerly aspect, as shown, when viewed in a frame of reference travelling with the cloud system. The ascent of the warm (red) flow is part of a thermally direct circulation and the flow accelerates as it rises, to give a jet maximum (J) at upper levels, consistent with conversion of potential energy into kinetic energy.

The blue CCB flow, which forms as the cyclone continues to develop, originates at low levels ahead of the warm front and gives rise to the cloud head. As the blue flow travels around the northern side of the cyclone centre, it ascends and fans out. The cloud shield generated by the blue flow has a characteristic convex-shaped leading edge: hence the name

'cloud head'. The emergence of the blue flow and its cloud head is associated with a second upper-level jet maximum, which is located just upwind of the dry slot. The ascent of the relatively cold air in the blue flow is part of a thermally indirect circulation in the exit region of this second jet. Thus, the frontal cyclone goes through a characteristic evolution in which the precipitation generated in its earlier stage is associated with ascending warm air (the red WCB flow), whilst the precipitation generated in the later stages is increasingly due to the ascent of cold air (the blue CCB flow) moistened to some extent by evaporation of precipitation falling from the overrunning warm air.

Fig 9 shows an analysis of relative-flow within $\theta_w$-surfaces applicable to the penultimate frame of the image sequence in Fig 8. It corresponds to Stage 2 in the life- cycle model in Fig 3. Figures 9(a), (b) and (c) show the flow inside the cloud head; air with $\theta_w$ = 9 and 10C can be identified with part of the CCB whilst air with $\theta_w$ = 11C is W2 air peeling off from the WCB. These $\theta_w$-surfaces should be visualised as stacked one above the other near the top of the cloud head ((a) above (b) above (c)). The leading edges of these flows are marked by wavy lines. Each of the wavy lines and the diffluent flow behind them are reproduced in Fig 9(d) to show the overall emerging-flow pattern at the top of the cloud head. The overlying flow in the stippled area of Fig 9(d) is the main warm-conveyor-belt flow, W1, associated with the polar-front cloud band. Vertical air velocities in the cloud head cannot be inferred quantitatively from these diagrams. This is because the $\theta_w$-surfaces were distorting with time as they began to wrap around the cyclone centre. The main point of Fig 9 is not to show the vertical air motion but, rather, to illustrate the origin and diffluent nature of the precipitation-generating flows within the cloud head.

The radar imagery in Fig 10 shows the typical pattern of precipitation associated with a cloud head. Although this is a different event from that represented in Figs 8 and 9, the situation is similar: a band of high frontal cloud extended from France to the North Sea, with a cloud head over southern Britain north of a cyclone centred near Brittany. The pattern of the cloud-head precipitation resembles that of the cloud itself except that the outer boundary of the surface precipitation is up to 100km inside the outer boundary of the cloud aloft. This is due to evaporation within dry air that descends beneath the outer edge of the cloud head. The tops of cloud and precipitation are typically at 2 to 3km at the inner (southern) edge of a cloud head and they rise to 6 or 7km towards the outer (northwestern) boundary (Fig 11).

A characteristic feature of the inner boundary of many cloud heads is a narrow and rather two-dimensional, though gently curved, rainband associated with a rope-like cloud line with tops at or below 3km (eg Monk and Bader 1988). It can be seen in the cloud and precipitation patterns in Figs 10, and 11, and it is sketched at hourly intervals in Fig 12 to show its persistence and movement. It is collocated with the bent-back front and, superficially in terms of its dimensions and sharpness, it resembles narrow cold-frontal rainbands and line convection as reviewed by Browning (1990). Although parts of bent-back fronts do indeed behave as cold fronts, narrow rainbands are sometimes observed (as in Fig 12) to extend into the stationary or warm-frontal parts of the bent-back fronts. In such circumstances the narrow rainband cannot be due to the density current mechanism proposed for narrow cold-frontal rainbands, eg Carbone (1982) and Hobbs and Persson (1982).

More complex sub-structure may also be observed in association with cloud heads. Parallel cloud lines about 10km apart are occasionally seen during rapid cyclogenesis at the

top of the cloud head, extending at right angles from the position of the bent-back front. The cause of these lines is not properly understood. Shutts (1990) suggests that they may be due to some form of marginally unstable roll instability associated with the intense frontal vertical wind shear within the cloud head. Thunderstorms are also a fairly common occurrence close to the bent-back front, especially at times of rapid cyclogenesis because this is a region characterised by strong potential instability where the intrusion of dry air with low $\theta_w$ overruns warm-conveyor-belt air. The nature and role of this 'dry intrusion' is our next topic.

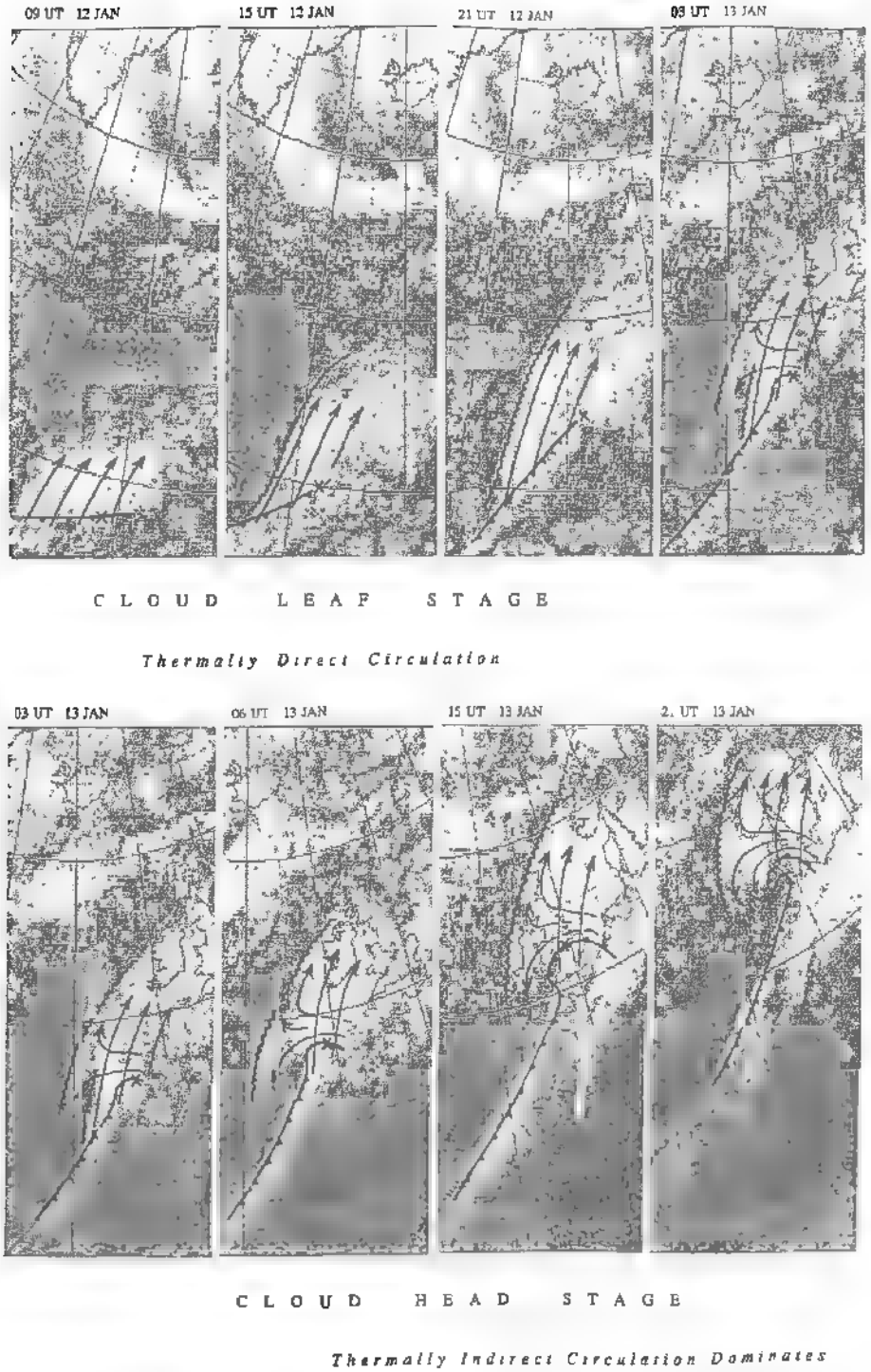


Fig.8 (Original figure in colour) Satellite sequence showing the development of a frontal cyclone. The sequence of mainly 6-hourly infra-red images (white represents the coldest/highest clouds) shows the evolution from the early stage of the cyclone, characterized by a 'leaf cloud' with a smooth s-shaped edge, to the mature stage with a well-formed 'cloud head'. Superimposed on the imagery are the positions of the cyclone centre (X), 300-mb jet cores (J), surface fronts (black line), edges of cloud leaf and cloud head (scalloped lines) and the principal cloud-producing flows (red and blue) drawn relative to the moving cyclone system. (Browning 1994).

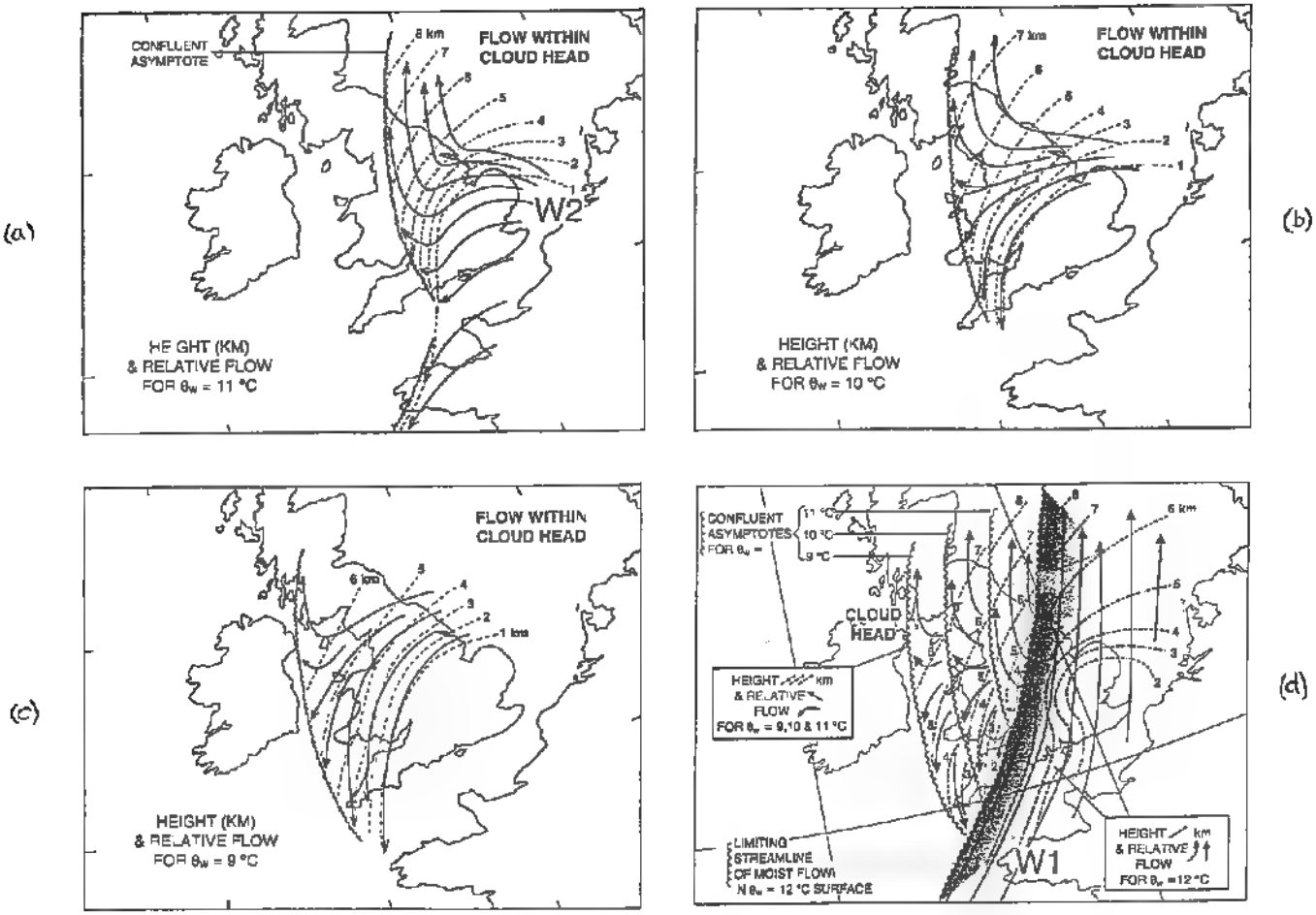


Fig.9 Model-derived flow in moist-isentropic surfaces relative to the cyclone in Fig 8 (at 15 UTC 13 Jan). The selected $\theta_w$-surfaces show (a) the W2 flow at the top of the cloud head and (b and c) the upper part of the CCB flow; (d) shows the superposition of the flow patterns from (a), (b) and (c) where the flows emerge at the top of the cloud head, plus the cloudy part of the W1 flow. (Browning and Roberts 1994).

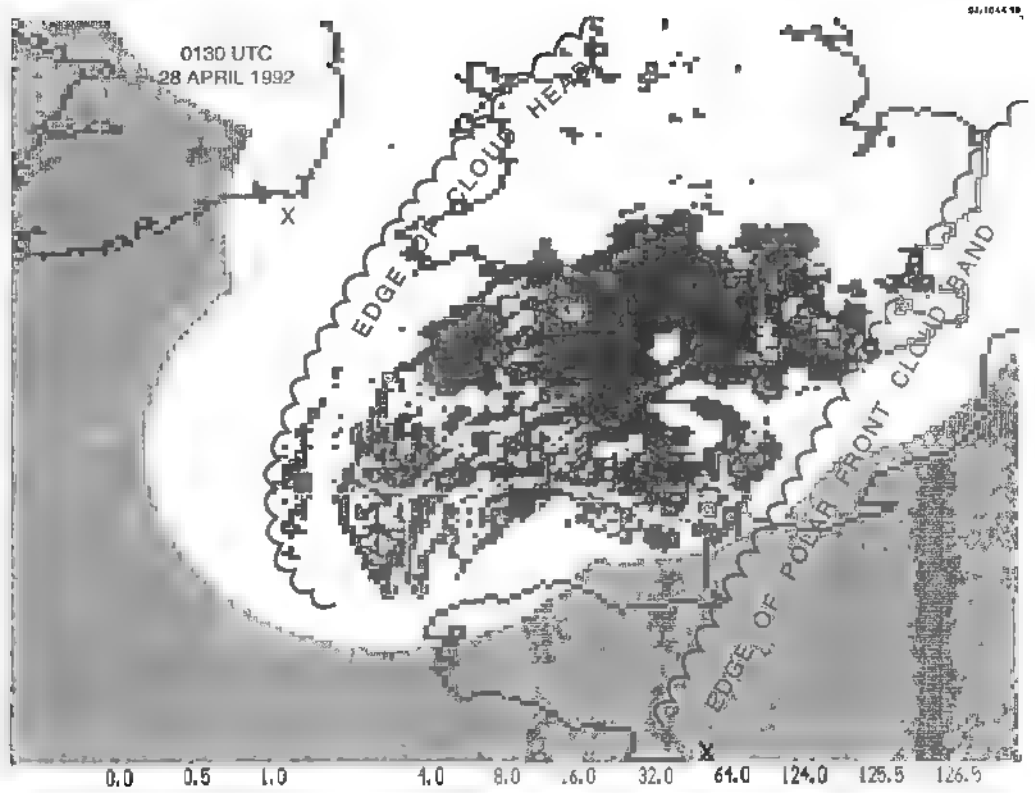


Fig.10 (Original in colour) Weather radar network display showing the pattern of precipitation associated with a cloud head. The long arc of yellow and orange echoes near the southern boundary of the precipitation is associated with the narrow band of heavy rain, only 2 to 3 km deep, sketched in Figs 11 and 12. Also indicated are the locations of the cyclone centre (L) and the poleward boundaries of the cloud head and polar-front cloud band (scalloped lines). A cross-section through a similar cloud system along a line corresponding approximately to XX is shown in Fig.11.

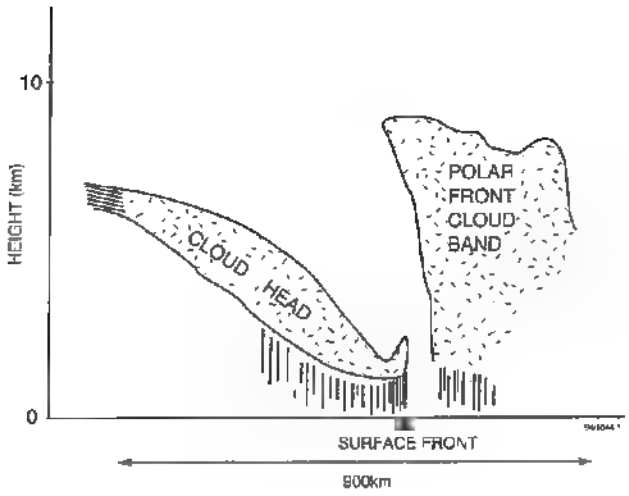


Fig.11 Outline of cloud boundaries across a rapidly deepening cyclone, inferred from cloud-top temperatures and numerical model thermal structure (After Shutts 1990 but with descriptive labels added to relate it to features described in this review). The base of the cloud head may sometimes be lower than indicated here.

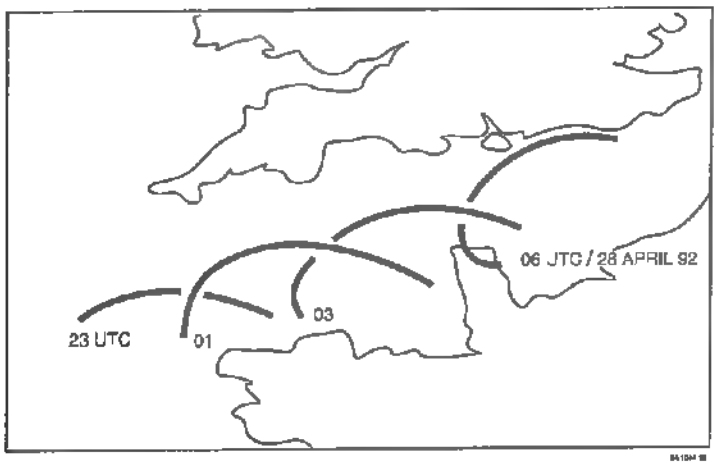


Fig.12 Progression of the bent-back front, as inferred from successive positions of the narrow rainband portrayed in Fig. 10 near the southern boundary of the cloud-head precipitation.

## 4. The dry intrusion

### 4.1 Upper-level origin of the dry air and the overrunning process

The notion of the dry intrusion as a key part of the cyclone structure responsible for the satellite-detected dry slot has already been introduced in Sec 2(b) above, and is embodied in the conceptual model in Fig 6. The source of the dry-intrusion air is to be found upwind of the cyclone in the upper troposphere and lower stratosphere in the region of a tropopause fold. The descent of such air in association with tropopause folding is well known following the work of Reed (1955) and Danielsen (1964). Danielsen's 3-D visualization is reproduced in Fig 13 which shows that the dry airstream cannot be approximated as a narrow belt-like flow; rather the upper-level air fans out over a very large area as it enters the lower troposphere. Only part of this dry airstream enters the region of the dry slot in the form of a dry intrusion as shown in Fig 6(c). There is some ambiguity over the use of the term dry intrusion: occasionally it is used loosely to describe the entire dry airstream as detected in satellite water vapour imagery well upstream of the cyclone. At other times the term is used specifically to describe the portion of the dry airstream that actually intrudes into the dry slot close to the cyclone centre. We shall adhere to the latter usage in this review.

The pattern of relative flow in Fig 13 looks deceptively simple but it has been carefully drawn to reveal several interesting facets of the overall dry airstream, part of which feeds the dry intrusion. Starting our description on the left side of the diagram, some of the dry air, upon reaching the lower troposphere, gets left behind and flows rearwards ahead of the warm front associated with the next cyclone in the sequence. Such dry air is often

encountered in and beneath a warm frontal zone; it is moistened by the evaporation of precipitation falling into it and it develops into the next cyclone's cold conveyor belt. In the middle portion of Fig 13, in the region of the first cyclone's trailing cold front, the dry airstream often reaches the ground as the descending limb of an ana-cold frontal circulation (see Fig 8.8 of Browning 1990). The portion of the dry airstream that becomes the dry intrusion is the set of 5 arrows on the right-hand side of Fig 13 which are shown overrunning the surface fronts. This air is often very dry because of its history of descent but by the time it gets to this position it is re-ascending within the dry slot.

Fig 14 shows analyses of surface pressure and wet-bulb potential temperature superimposed on the Meteosat water vapour (WV) imagery for the occasion depicted in Fig 10 but at a slightly later stage in the process of frontal fracture. High radiance values in the WV image show the presence of dry air in the middle and upper troposphere. The highest radiances (dark in Fig 14) show the penetration of the dry intrusion into the dry slot ahead of the cyclone centre. The frontal analysis in Fig 14(a) shows a diffuse surface cold front (dashed line) where the dry intrusion overruns it, as in the conceptual model in Fig 6. This lies behind a tongue of high-$\theta_w$ air (Fig 14 (b)) associated with a shallow moist zone (the W2 flow) that was capped by the dry intrusion. The leading edge of the dry intrusion is depicted in Fig 14(a) by open cold frontal symbols and it corresponds to what Browning and Monk (1980) refer to as an upper cold front. However, they pointed out that this feature is often better described as a humidity or $\theta_w$-front and, as on this occasion, is not necessarily associated with significant cold frontal baroclinity.

This point is illustrated by a cross-section along the axis of the dry intrusion (Fig 15), which shows that the actual cold ($\theta$) frontal zone aloft is located well behind (rather than at) the upper cold $\theta_w$-front. The cold $\theta$-front is a dynamically induced phenomenon due to differential subsidence of the upper-level dry air. The cold $\theta_w$-front is the true front in airmass terms and is the more significant front in terms of weather. Given sufficient local lifting, the cold $\theta_w$-front also manifests itself as a cold $\theta$-front. Upper cold $\theta_w$-fronts are ubiquitous features of developing cyclones and have been variously described as moisture fronts (Mass and Schultz 1993) and cold fronts aloft (Hobbs et al 1990), as well as upper cold fronts. There is a tendency to emphasise the differences between these fronts but we would prefer to stress the key factor they have in common, namely the role of the dry intrusion in generating what is strictly an upper cold $\theta_w$-front. With this amended terminology, the observations conform to the simple split-front model of Browning and Monk (1980) - see Fig 16. The word 'split' in this model refers to the upper part of the cold $\theta_w$-front running ahead of the surface cold front. In between there is a region which Browning and Monk refer to as the Shallow Moist Zone (SMZ). An SMZ is often encountered on the warm side of a bent-back front as shown in the conceptual model in Fig 6. In the kind of system shown in Fig 7 the SMZ may be a more extensive feature.

### 4.2 The association of high potential vorticity with the dry intrusion

Since the early work of Reed and Danielsen it has been known that part of the dry airstream that descends from near tropopause level during tropopause-folding events brings with it values of potential vorticity (PV) characteristic of the lower stratosphere. The output from operational forecast models shows clearly how, during the development of vigorous

cyclones, the dry intrusions sometimes contain air with PV of 2 or more PV units (eg Uccellini et al 1985, Young et al 1987). A value of 2 PV units is regarded as defining the dynamical tropopause: broadly speaking, it discriminates the generally high-PV stratospheric air from the generally low-PV tropospheric air. Admittedly, there are regions of high PV generated in situ within the troposphere by diabatic effects but these are within the moist air and, given NWP model output of sufficient resolution, can be distinguished from the high-PV air in the dry intrusion. As explained by Hoskins et al (1985), it is the overrunning of such high-PV air above a low-level baroclinic zone that leads to cyclogenesis and so it comes as no surprise that dry intrusions such as the one in Fig 14 are most in evidence at the stage of rapid cyclogenesis.

The example we have chosen in order to illustrate the occurrence of high PV within a dry intrusion is more complex than the dry intrusion case described in Fig 14; in fact it corresponds to a different category of cyclone similar to Young's 'diffluent flow' sub-category of frontal cyclone (see Figs 2(c) and 7). This example has been chosen because of the availability of high-resolution diagnostics from a recent case study using a mesoscale model (Browning and Golding 1995). The results for this case are shown in Figs 17 to 20 and they are interesting in that they reveal strong mesoscale substructure: a single dry intrusion splits into two smaller ones and each becomes associated with an identifiable dry slot and notable cyclonic events.

Fig 17 shows successive 3-hourly positions of the dry slot seen in WV imagery. The dry slot grew and became elongated within a strong deformation zone before splitting into two. One of the resulting dry slots then travelled NEwards across Scotland in association

with a rapidly deepening mesoscale cyclone. The other travelled eastwards accompanied by a sharp trough and tornadic squall line. The relative humidity pattern at 3km (Fig 18) obtained from the mesoscale model shows a mesoscale dry intrusion associated with each of the satellite-detected dry slots. Time sequences of model diagnostics on an appropriate isentropic surface, for the southern dry intrusion, show that the dry intrusion was characterised by a region of dry air (Fig 19(a)) and a collocated region of high PV (Fig 19(b)) which descended from about 3 to 1km within 6 hours. The fact that the high PV is generally associated with dry intrusions has led Mansfield (1994) to recommend evaluating NWP model performance by comparing model-derived PV patterns with WV imagery.

The vertical section in Fig 20 shows that the dry intrusion was a narrow filament extending down from a tropopause at 6km. Parts of the dry intrusion below 3km had a relative humidity less than 30% and a PV as high as 2 PV units. The moist airmass into which the dry intrusion was penetrating also had pockets of high PV, due to the locally-generated diabatic effects; however, continuity in the analysis made it possible to attribute the PV features to the appropriate level of origin. Although low-$\theta_w$ air in the dry intrusion was overrunning high-$\theta_w$ air in the lowest kilometre or so, Fig 20 shows that it was also partly undercutting the deep mass of cloudy high-$\theta_w$ air associated with the warm conveyor belt. This often happens, in which case the satellite imagery is not capable of detecting the full extent of the dry intrusion.

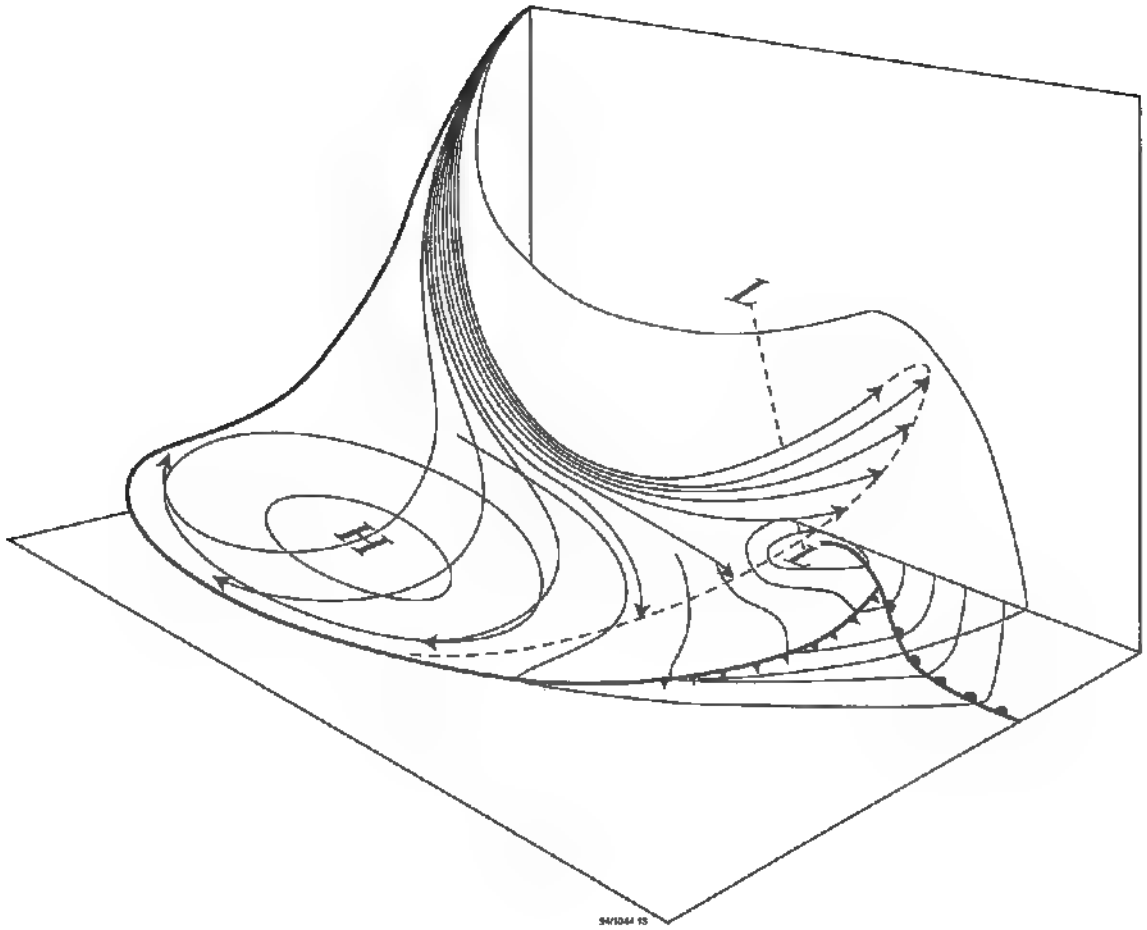


Fig.13 Trajectories of extruded stratospheric air drawn within a curved isentropic surface. The surface is shown sloping from a point near a tropopause fold down to the ground. Trajectories reach all the way to the ground in the left part of the diagram but not in the right-hand part, where they overrun the surface fronts (Danielsen 1964).

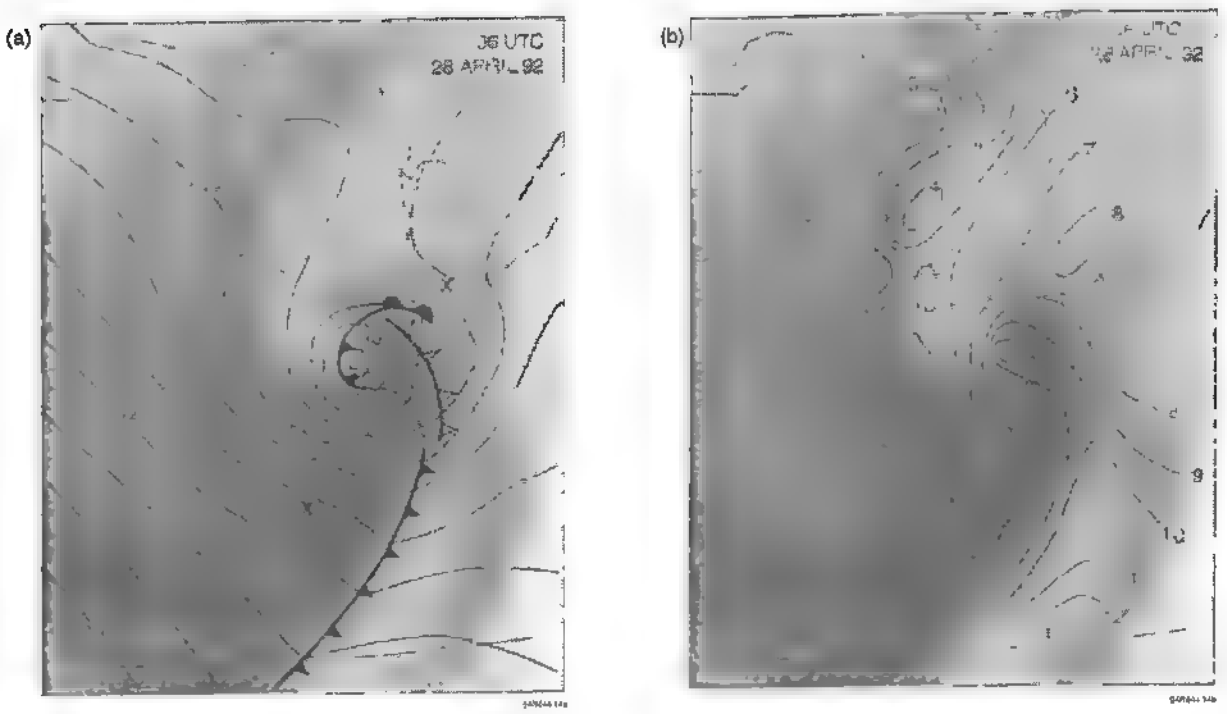


Fig.14 Analyses and satellite imagery for a rapidly developing cyclone: (a) msl pressure and frontal analysis, (b) surface $\theta_w$, both superimposed on water vapour imagery showing the dry intrusion (dark zone) penetrating ahead of the cyclone centre. Surface fronts are depicted with solid markings; the upper cold $\theta_w$-front is shown with open barbs. The diffuse portion of the surface cold front in the region of frontal fracture is shown dashed. XX gives the location of the section in Fig 15.

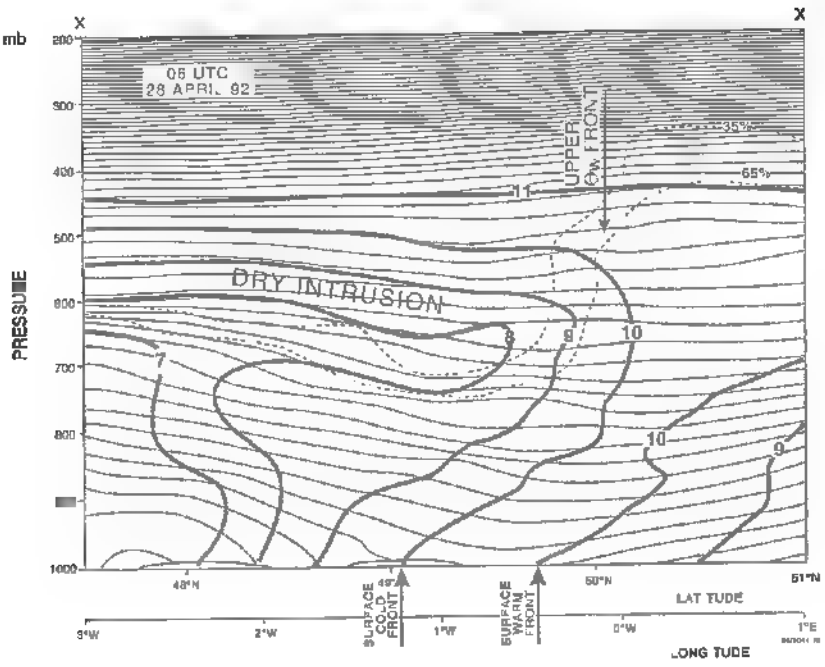


Fig.15 Vertical section along XX in Fig.14 showing $\theta_w$ (thick solid lines at 1°C intervals), $\theta$ (thin solid lines at 1°C intervals) and relative humidity (dashed lines for 65% and 35%), as obtained from a 12 -h mesoscale model forecast with assimilation of soundings from a mesoscale array of dropwindsondes (Courtesy of S Ballard and C Davitt). Note that the surface cold front, marking the leading edge of a diffuse $\theta_w$-gradient is overrun by dry-intrusion air with low $\theta_w$ which gives an upper $\theta_w$-front more than 100 km ahead of the surface cold front. An upper cold $\theta$-frontal zone does not accompany the upper $\theta_w$-front here but, rather, lags behind.

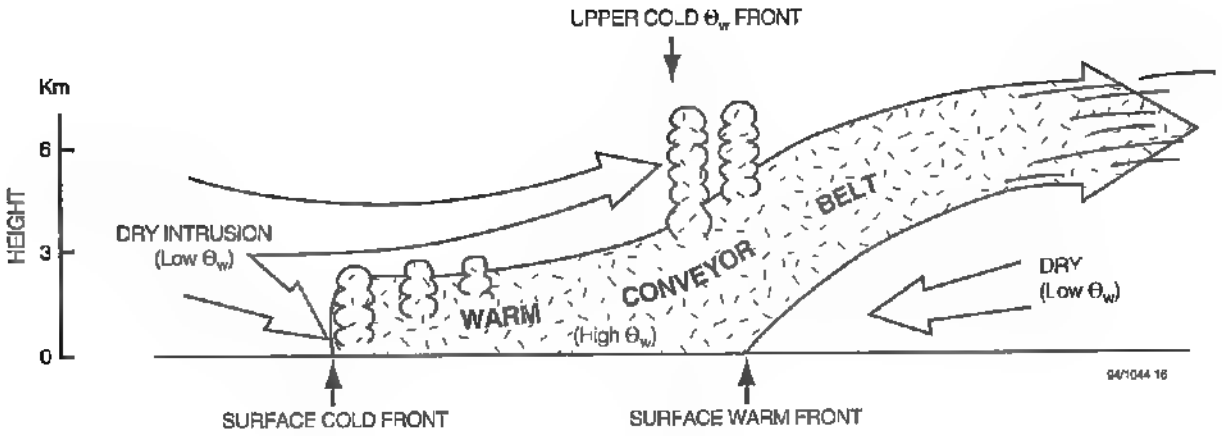


Fig.16 Simple model of a kata-cold frontal situation in which dry air with low $\theta_w$ overruns a shallow moist zone of high-$\theta_w$ air (Adapted from Browning and Monk 1982).

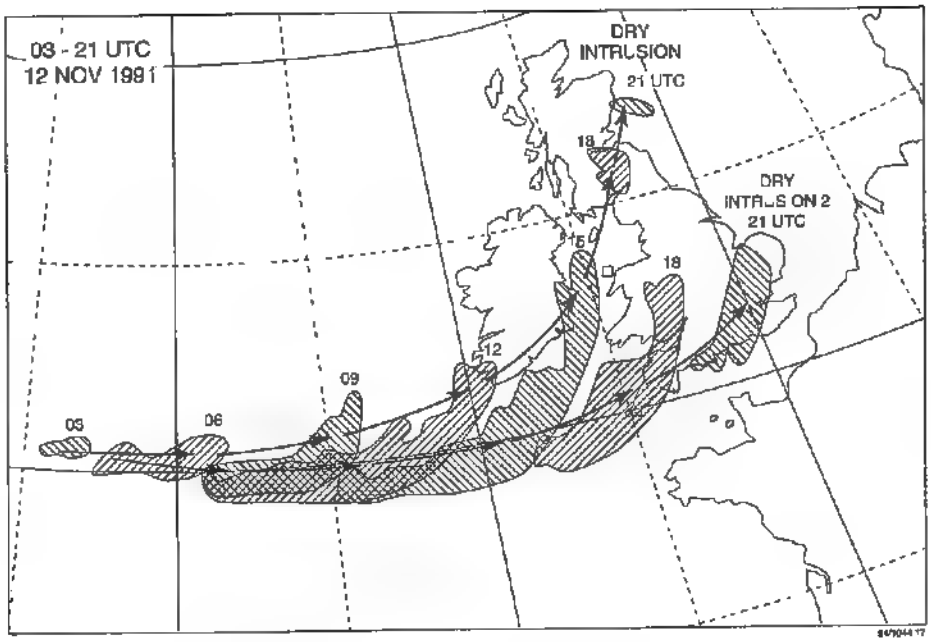


Fig.17 Tracings of the dark zone in Meteosat water vapour imagery at 3-h intervals, showing the tracks of two pockets of dry-intrusion air (Browning and Golding 1995).

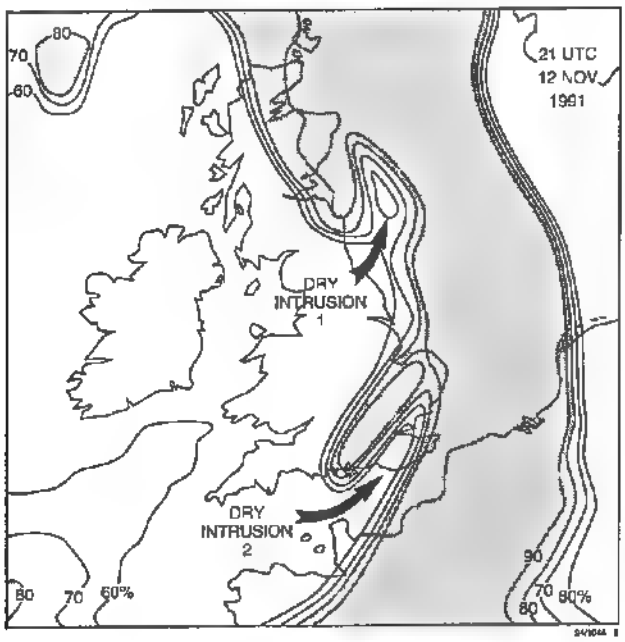


Fig.18 Mesoscale model forecast for the case shown in Fig 17, at 21 UTC, initialised from operational limited-area model fields at 12 UTC, showing relative humidity at 3 km above msl. Contours are for 60, 70, 80 and 90%. Areas in excess of 90% are shaded. The two dry intrusions seen here are also evident in the satellite imagery in Fig.17. (Browning and Golding 1995).

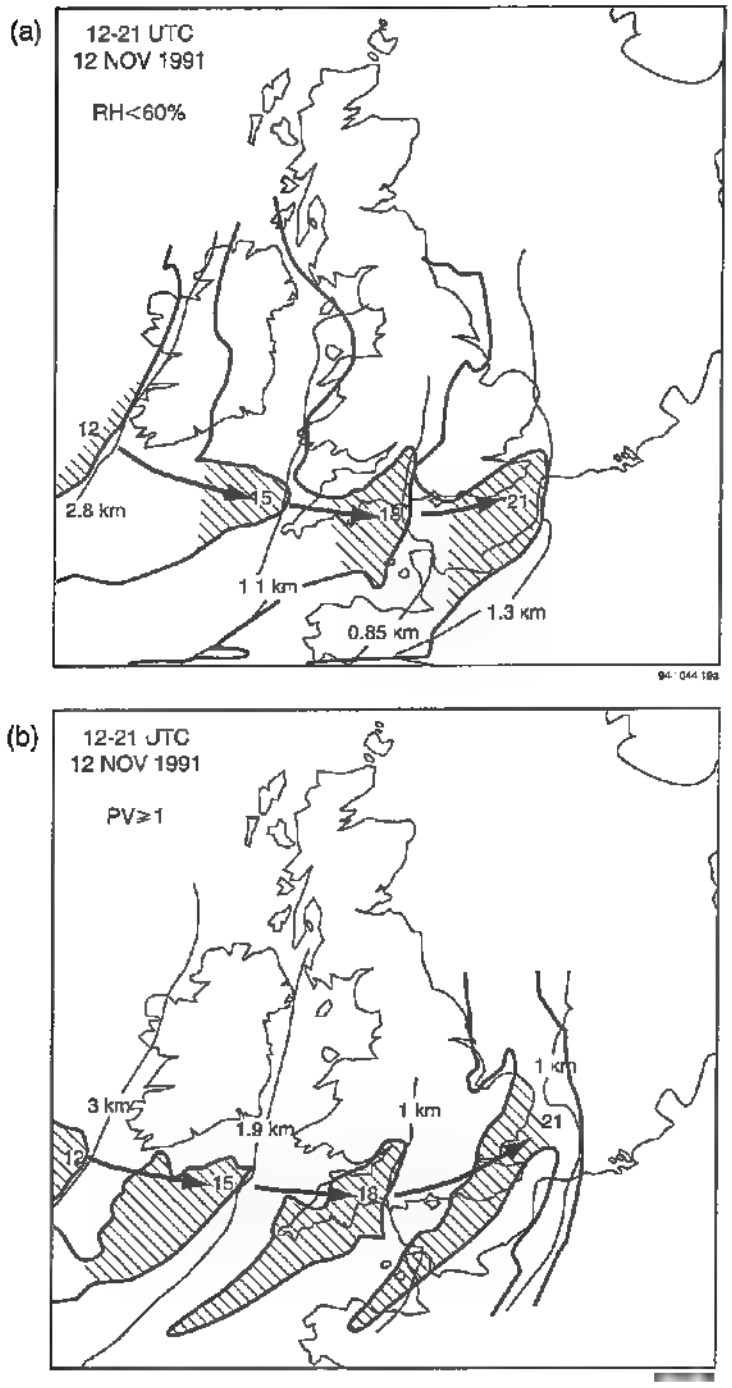


Fig.19 Three-hourly plots for the case shown in Fig 17, depicting the evolution within Dry Intrusion 2 of (a) relative humidity <60% and (b) PV $\geq$ 1 within the 16°C isentropic surface, as depicted by a mesoscale model. The dry and high-PV features are highlighted by shading, (the part of the high-PV region at 21 UTC that is unshaded corresponds to diabatically - generated PV originating at low levels). Also shown (thin lines) are height contours through the lowest parts of these features. (Browning and Golding 1995).

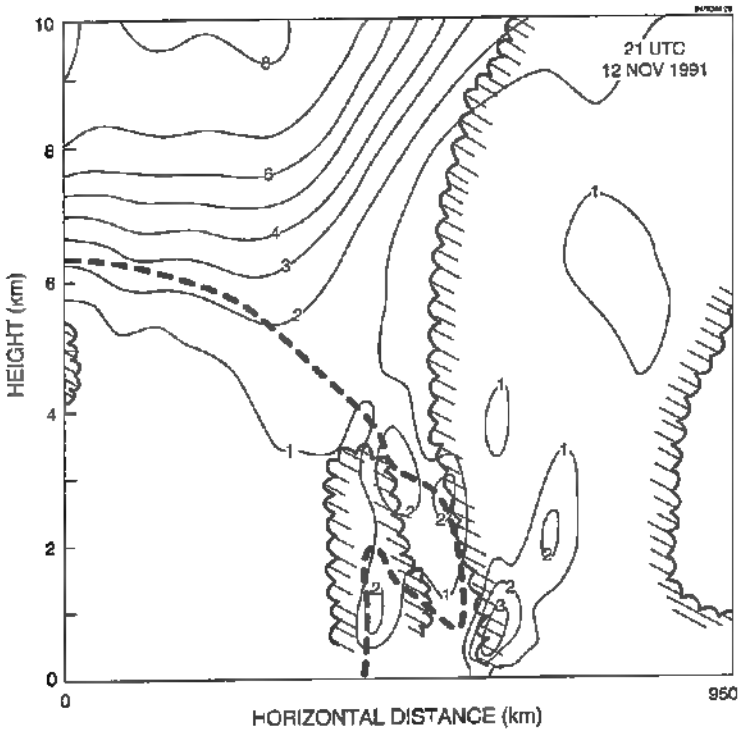


Fig.20 Forecast cross-section along the south coast of England, from a mesoscale model, for the case shown in Fig 17, depicting potential vorticity (solid contours at intervals of 1 PV unit), the $\theta_w$ = 7C isopleth (dashed line) and the cloud boundary (scalloped). (Browning and Golding 1995).

## 5. Mesoscale sub-structure of surface cold fronts in the region of the dry intrusion

This section is not about classical ana-cold fronts that occur sometimes a long way from the cyclone centre: these have been dealt with in the review by Browning (1990) under the heading of warm conveyor belts undergoing 'rearward-sloping ascent'. Rather, it is about the kata-cold fronts that occur, often close to the cyclone centre, where the low-$\theta_w$ dry-intrusion air overruns the warm-conveyor-belt flow W2 as in the split-front model in Fig 16. This type of front was also discussed in the 1990 review, under the category of warm conveyor belts undergoing 'forward-sloping ascent'. However, more recent research has revealed a rich variety of mesoscale structure associated with such fronts. In this section we examine the structure of the surface cold-frontal part of the split front in Fig 16, and we show that the surface cold front may itself be characterised by multiple structure.

We illustrate the sub-structure using a combination of satellite data and soundings from a mesoscale array of about 60 dropwindsondes. The sondes were released during the FRONTS 92 experiment in the cold-frontal region of a developing frontal cyclone over the eastern Atlantic. The satellite pictures in Fig 21 show a cloud head south of Ireland and a polar-front cloud band extending from Biscay to southern England. The distinction between these two cloud features is clearest in the infra-red image (Fig 21(a)) which shows that the tops in the cloud head are lower than those in the polar-front cloud band. At this early stage of cyclogenesis the dry intrusion had not yet penetrated fully into the system and the dry slot is not yet well formed in the infra-red image. The area we wish to focus on is the region of low-level cloud lines to the southwest of the cloud head. These appear insignificant in the infra-red image because they are so low, but they are relatively bright in the visible image

(Fig 21(b)). According to the detailed analysis in Browning et al (1995) they are associated with two surface cold fronts (CF1 and CF2) plus other similar but weaker cold frontal sub-structure: we now summarize some of their results.

Fig 22 (a, b and c) shows relative-flow analyses within isentropic surfaces ($\theta$=20, $\theta$=10 and $\theta_w$=7C) behind and within the cloud head. The cloud head (stippled) is shown in each of the panels together with surface positions of CF1 and/or CF2. The right-hand panel (c) shows a flow characterizing the cloud head. The left-hand panels show flow in the dry air just above (top panel (a)) and just beneath (bottom panel (b)) the shallow southwestern end of the cloud head. The NNEly relative flow beneath the cloud head descends to the surface behind CF2. The NNWly relative flow just above the cloud head descends close to the surface at CF1; some of it penetrates to the surface (hatched area along CF1) and some overruns it and begins to re-ascend as a dry intrusion.

Figs 23 (a) and (b) show a vertical section of relative humidity and $\theta_w$ constructed from 17 dropsondes along AB in Fig 22(c). The broad-scale pattern is of dry, low-$\theta_w$ air overrunning a moist boundary layer and penetrating towards the surface in places. The satellite water vapour imagery showed two zones of dry air plunging downwards as shown schematically by the two bold arrows in Fig 23(b). The leading edge of one of these corresponds to the $\theta$=10C flow undercutting the cloud head; the other corresponds to the $\theta$=20C flow overrunning the southwestern tip of the cloud head (cf Fig 22(a)). At the top of the boundary layer, mesoscale circulations associated with each of these dry intrusions distort the strong vertical gradient of humidity to produce fingers of dry and moist air (dry axes are shown dashed in Fig 23 (a)). Actually these fingers were extensive into the plane of the

diagram and should be regarded as being interpenetrating dry and moist laminae, with a front-normal slope of 1 in 60. Although the water vapour imagery could resolve only two distinct dry zones, each of them led to a multiply-laminated mesoscale structure, as evidenced by the multiple dashed lines in Fig 23(a).

Corresponding fine structure existed in the wind field and Fig 23(c) shows the lamination in vertical shear of the front-parallel component which, in the case of the geometry of these features, can be used as a proxy for (vertical) vorticity. It is possible that these vortex sheets or shear layers were due to pre-existing unresolved mesoscale blobbiness in the pattern of vorticity at tropopause level which was then stretched out into thin laminae by the deformation field as the dry air descended. Alternatively they may have been due to mesoscale instabilities such as conditional symmetric instability developing where the descending dry air encountered the moist boundary-layer air. Fig 23(c) suggests that both mechanisms could have been occurring: The shear layer extending down from the top left corner existed at high levels where it was entirely within the dry air, as well as extending to lower levels where it seems to have perturbed the interface between moist and dry air. The other shear layers in Fig 23(c) all appear to be closely confined to the vicinity of the interface between the dry descending air and the moist boundary-layer air. It may be significant that these laminations occur in the vicinity of a critical level (dashed curve in Fig 23(c)) where the component of the wind resolved along the direction of travel of the cyclone system was equal to the system velocity.

A detailed analysis of dropwindsonde data within a small area at the bottom right-hand corner of Fig 23 has been carried out to reveal the fine structure associated with one of the

surface cold fronts (CF1). Figs 24(a-c) show the resulting analyses of (a) relative humidity and cloud, (b) wet-bulb potential temperature and (c) transverse-front wind-component. The shaded areas in each panel draw attention to the narrow lamina of rearward-sloping moist (but mainly subsaturated) ascent just ahead of a corresponding lamina of forward-sloping dry (low-$\theta_w$) descent. Fig 24(d) shows that the interface between the two laminae corresponded to a shear layer characterised by a sub-critical Richardson Number indicative of ongoing shear-induced turbulent mixing. The surface position of the cold front occurred where this shear layer penetrated to the ground, immediately ahead of which it triggered a band of shallow convective cloud. This convection can be seen in Fig 24 (a) to have risen to a level between 2 and 2.5 km where there was a weak flow overtaking the front which carried the cloud debris ahead of the surface front.

The front in Fig 24 was a kata-cold front (Bergeron 1937) but this detailed analysis has shown that even at a kata-cold front, with dry-intrusion air overrunning it aloft, there may still be a hint of a small-scale ana-cold frontal circulation. Unlike in a fully developed classical ana-cold front, where air is peeled out of the boundary layer and ascends as a major precipitation-producing flow into the middle or upper troposphere, the slantwise ana-cold frontal ascent in Fig 24 is weak, shallow and, in this case, largely cloud-free. Without a very dense line of dropwindsondes it would have been unresolvable. Nevertheless it did exist and its very existence is thought-provoking. The writer used to think of kata- and ana-fronts as being quite distinct. Now it appears that pure kata-cold fronts and pure ana-cold fronts are the extremes of a continuous spectrum of structures, as sketched in Fig 25. The early development of a cloud head, before diabatic effects become important, may perhaps be interpreted in terms of a progression from (a) to (c) in Fig 25 due to the upward extrusion of

boundary-layer air under the influence of a region of high potential vorticity originating at upper levels.

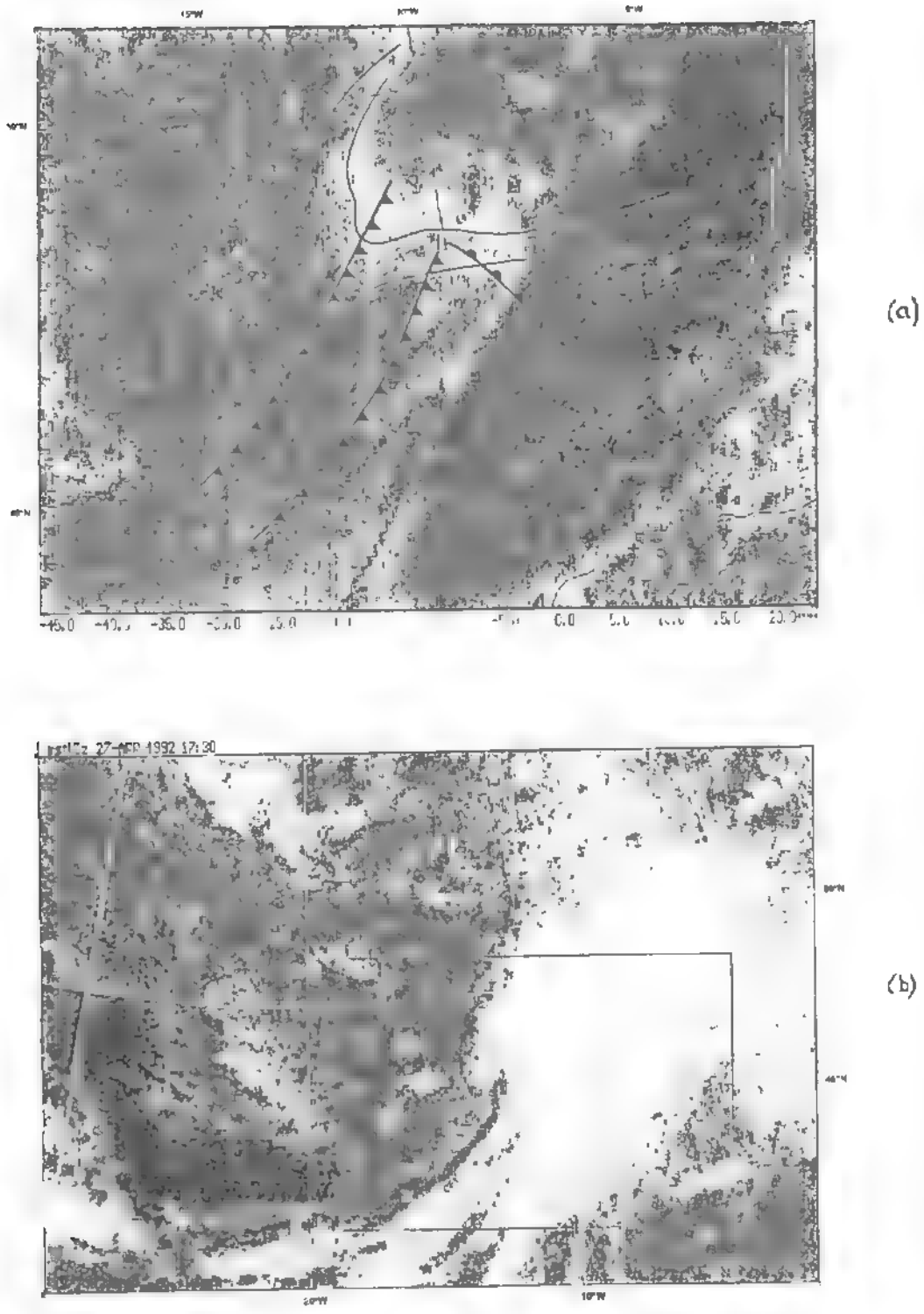


Fig.21 (a) Meteosat infra-red false-colour image, showing two cold fronts, CF1 and CF2, extending from the tip of a cloud head. Cloud-top temperatures (deg C) are given by the colour code along the bottom. (b) Meteosat visible image ½h before (a), with the same two cold fronts labelled. The frame shows the extent of the area covered in (a). (Browning et al 1995).

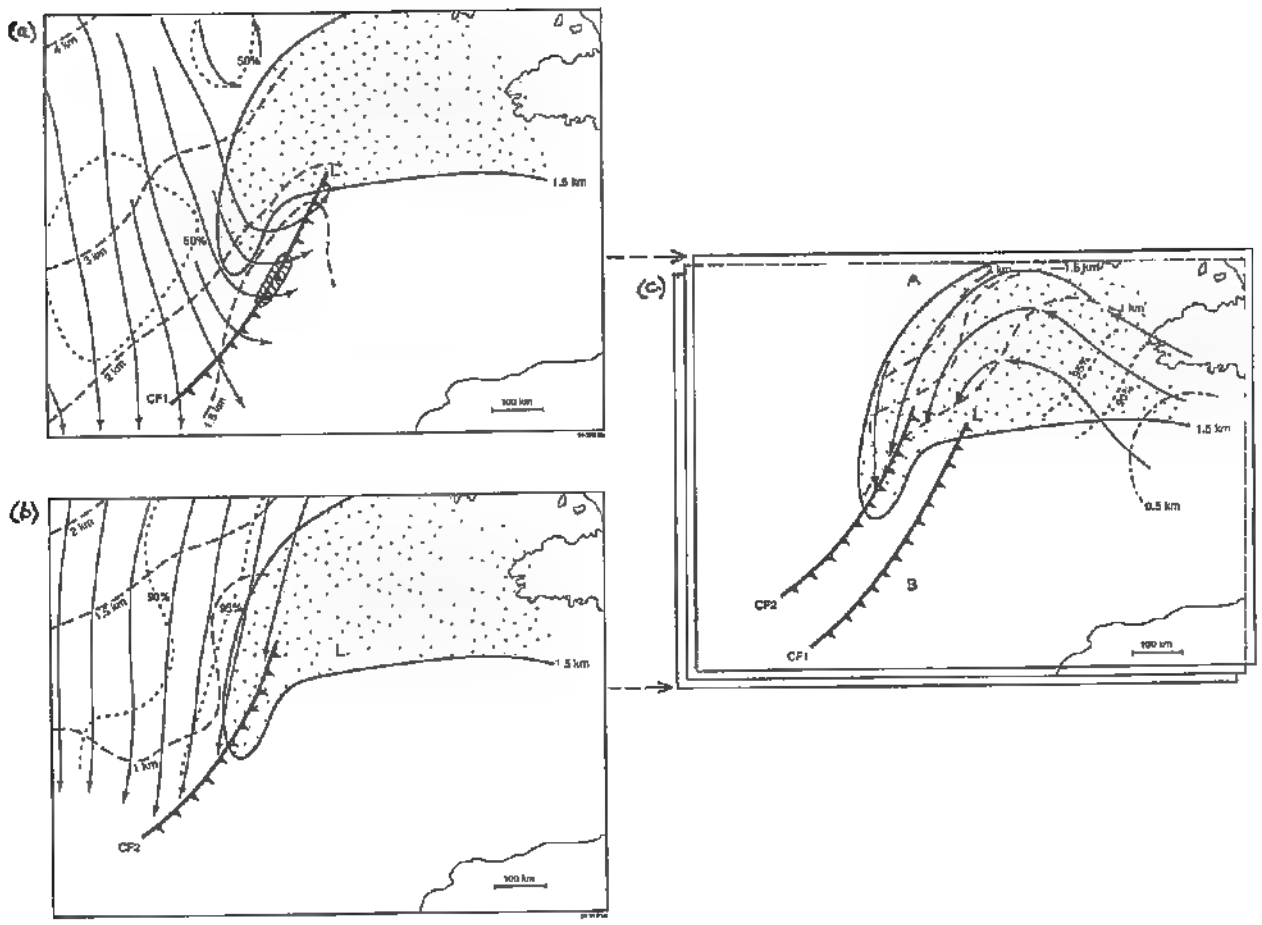


Fig.22 System-relative flows for the case shown in Fig 21, derived from dropwindsondes. The flows represent: (a) dry air in the $\theta$ = 20C surface mainly behind CF1, (b) dry air in the $\theta$ = 10C surface behind CF2 and (c) moist air in the $\theta_w$ = 7C surface within the cloud head. Part of the flow in (c) intrudes between the flows in (a) and (b). Dashed lines shows the heights of these surfaces. Dotted lines show relative humidity. Also shown are the position of the cyclone centre (L) and extent of moist air (RH > 90%) above 1.5 km associated with the cloud head (stippled shading). The 0.5 km base of a shallow layer of dry air beneath the warm frontal zone is denoted by the dot-dashed isopleth in (c). Another region, along CF1, where dry air penetrated downwards as far as 0.5 km is shown in (a) by hatched shading. AB in (c) shows the line of the cross-section in Fig.23. (Browning et al 1995).

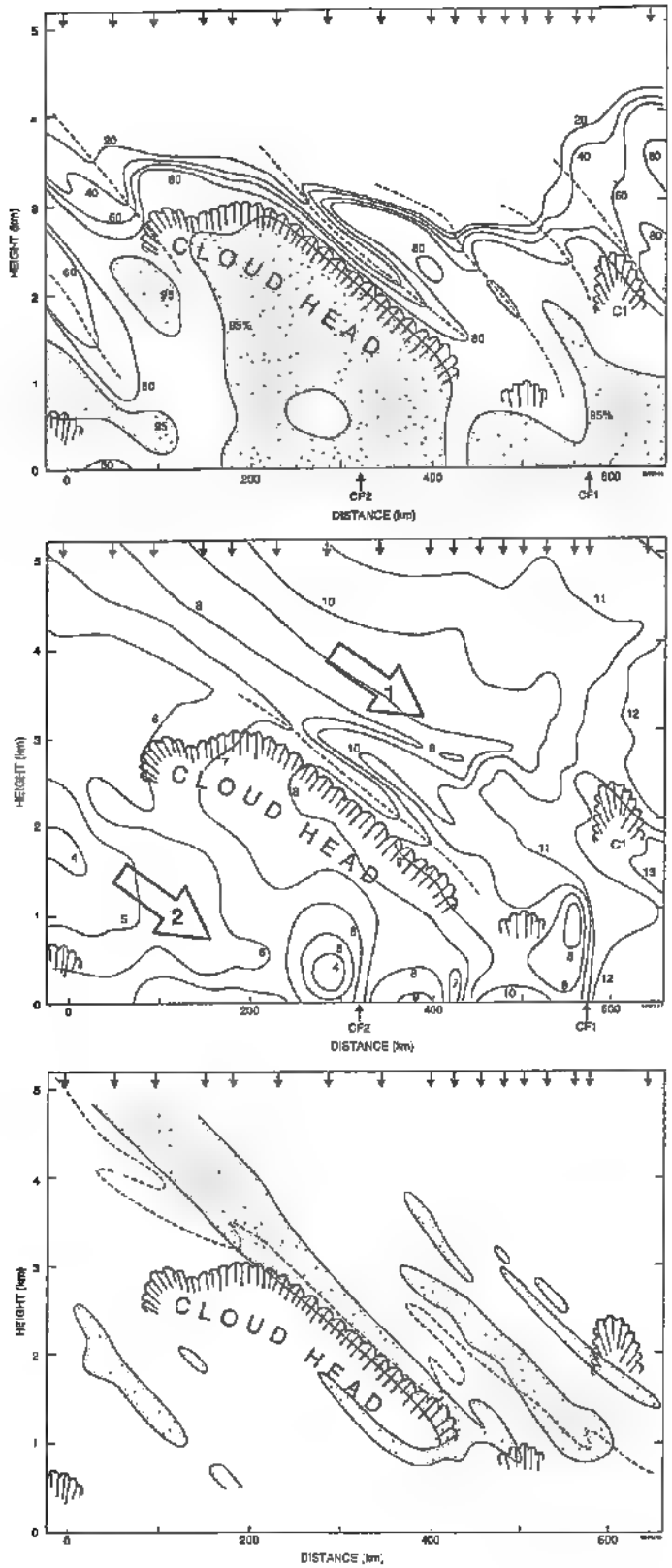


Fig.23 Cross-section along AB (see Fig.22(c)) derived from dropwindsondes (locations at top of figures) showing isopleths of (a) relative humidity (shaded above 95%), (b) wet-bulb potential temperature (isopleths at 1C intervals) and (c) vertical shear in the component of the wind resolved parallel to the cold fronts (stippled laminae show shear greater than 1 $ms^{-1}$ per 100 m). Cloud tops inferred from satellite imagery are shown in all three figures. The two large arrows labelled 1 and 2 in (b) draw attention to the two dry intrusions. The dashed curve in (c) shows a critical level (see text for definition). (Browning et al 1995).

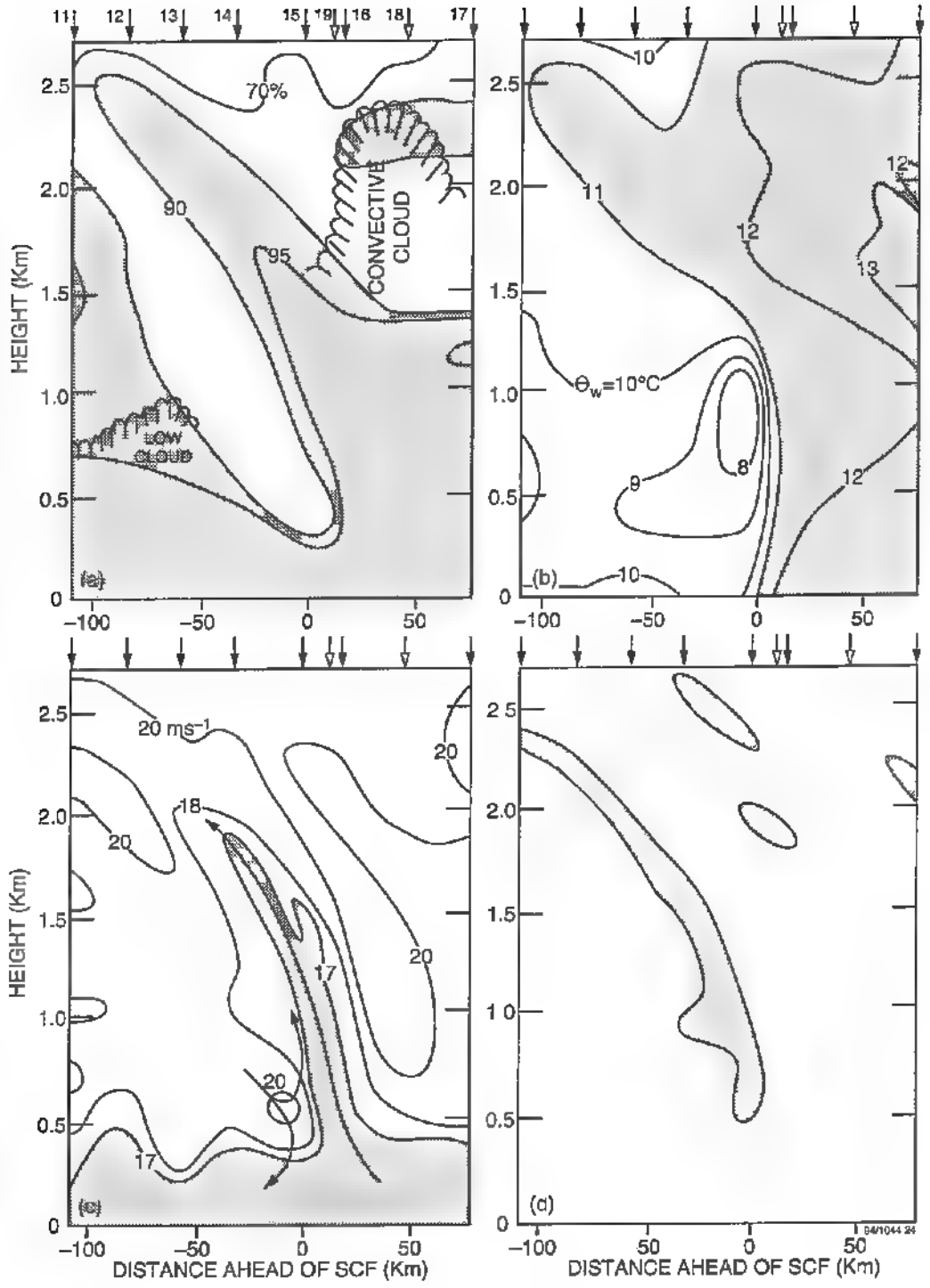


Fig.24 Cross-section through surface cold front CF1 along the southern part of AB in Fig 22(c) based on 9 dropwindsondes (see arrows at top of diagrams). The 4 panels show: (a) relative humidity (isopleths at 70, 90 and 95%, shaded above 90%) and cloud tops (derived from satellite), (b) wet-bulb potential temperature, $\theta_w$ (isopleths at 1C intervals, shaded above 11C), (c) front-normal wind component (isopleths at 17, 18 and 20 m s$^{-1}$, shaded below 17 m s$^{-1}$; velocity of front was between 17 and 18 m s$^{-1}$), and (d) Richardson Number less than ¼ measured over 20 mb layers. (Browning 1995).

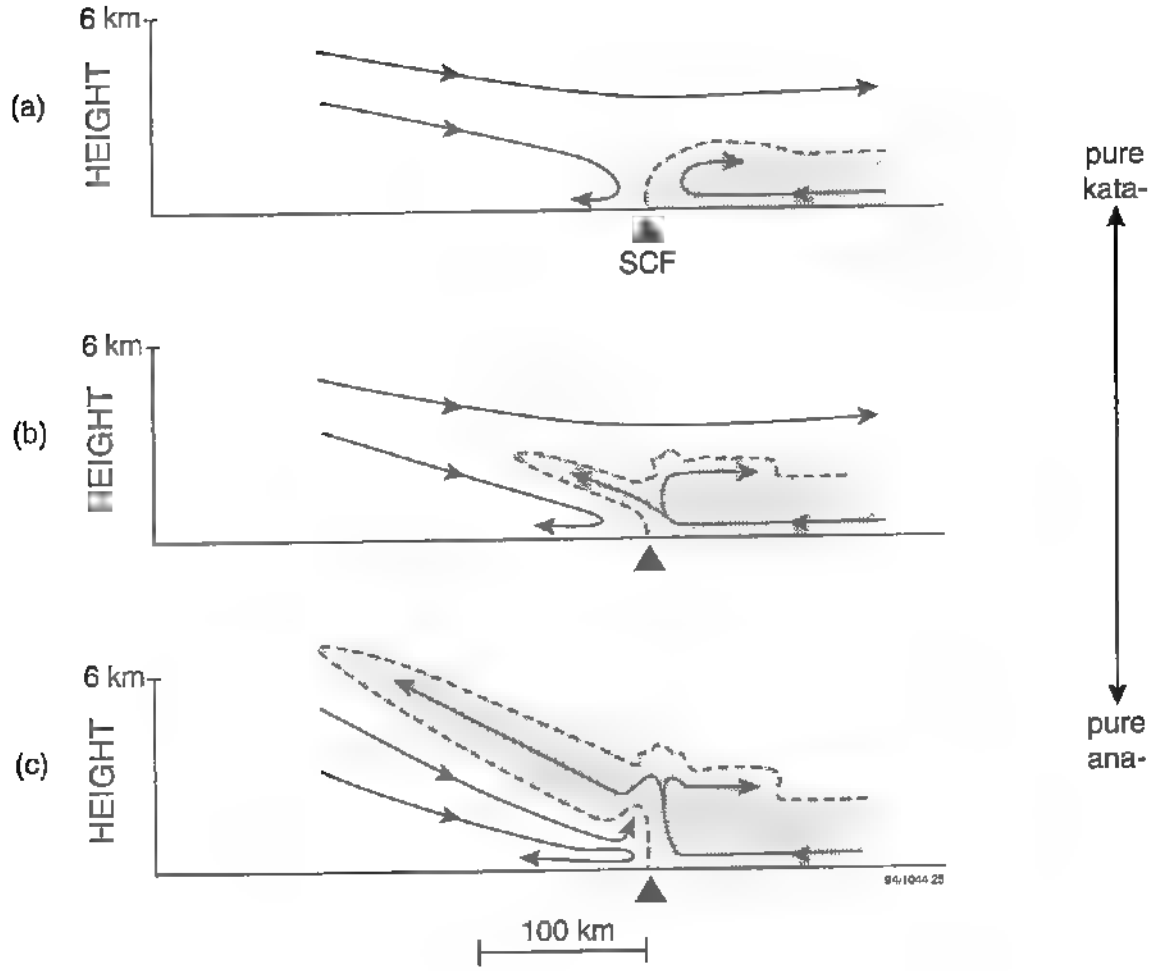


Fig. 25 Schematic cross-sectional representations of the spectrum of cold-front types, ranging from a pure kata-cold front to a pure ana-cold front. Arrows show transverse flow relative to the front. Stippled shading bounded by dashed contour represents boundary-layer or extruded boundary-layer air.

## 6. Outbreaks of convection associated with the dry intrusion

We have described in Sec. 4 how the dry intrusion, as it advances ahead of the centre of a developing cyclone, produces a dry slot detectable in the satellite imagery (eg Fig 14). We have also shown (see split front model in Fig 16) how this region is characterized by low-$\theta_w$ air overrunning a shallow moist zone characterized by high $\theta_w$, thereby leading to potential instability. The air, as it enters the region from the west, is usually convectively stable because of the adiabatic warming of the dry-intrusion air during its earlier descent, but within the dry slot it begins to ascend and eventually the potential instability may be realized in the form of convection. This is especially likely in association with a rapidly developing cyclone where the lifting is strong and/or, over certain continental (oceanic) areas in summer (winter), when there is substantial input of heat at the surface. The purpose of this section is to examine the location and nature of the resulting convection.

Fig 26 is an adaptation of the results of a composite study by Carr and Millard (1985) showing the location of severe convection-related weather events in relation to the pattern of cloud associated with a mature cyclone. A key feature of their study was the identification of the dry intrusion (arrow in Fig 26) which was responsible for the satellite-detected dry slot within a large comma-shaped cloud system. We interpret the overall comma cloud here as being the combination of cloud head and polar-front cloud band as described above, but the distinction between these two cloud features does not always exist. The numbers plotted in Fig 26 represent the percentage occurrence of severe weather events averaged over ten large zones. According to Carr and Millard, the high number of events associated with the polar-front cloud band occurred mainly close to the boundary with the dry intrusion. Thus our

estimate of the area most prone to severe convection is shown by the dashed envelope in Fig 26. In the central USA, where this study was conducted, 7% of the convection occurred within the dry slot itself; the rest occurred at its boundaries. Many convective lines were found to form in the dry slot and then to move eastward into (or to redefine the western edge of) the polar-front cloud band as they became severe.

An example of the formation of a dry slot in a rapidly developing cyclone, followed by the outbreak of convection within it, is shown in Fig 27. The analyses, at 2-hour intervals, show the leading edge of the dry intrusion (corresponding to the upper cold $\theta_w$-front) progressively overrunning the surface cold front. The first deep convective cells broke out within and just ahead of the dry intrusion a few hours after the formation of the dry slot. The cyclone centre was deepening rapidly but the fastest pressure falls occurred south of the centre where the intense convection was breaking out. A visualization by Hobbs et al (1990) of the outbreak of such a line of deep convection ahead of a dry intrusion is shown in Fig 28. The situation depicted here is essentially the same overrunning situation that is represented in the split-front model (Browning and Monk 1982) but the surface feature is referred to as a surface trough rather than a surface cold front. These surface features are often a source of confusion: in NW Europe they tend to have a small temperature drop and a somewhat larger drop in dew point but in the central USA, for which Fig 28 was derived, the local conditions can lead to a temperature rise behind the surface trough, to the west of the shallow moist zone.

The case described in Fig 27 was of deep convection from the surface. Often in NW Europe convection associated with the dry intrusion is limited to a shallow mid-tropospheric

layer. Fig 29 shows the development of convective clouds at 2-hour intervals ahead of an upper cold front associated with the leading edge of a dry intrusion. At time T the upper cold front was approaching Brest, at which time it was about 200km ahead of the surface cold front and just beginning to overrun the warm front. A sounding from Brest (B) at the southern end of the line of convection shows that the convection was associated with the buoyant ascent of air parcels from the 800-700mb layer just above the warm frontal zone.

Convection breaking out within the dry slot has a tendency to form in lines. Occasionally, especially in the central USA, these become intense squall lines. More often in maritime parts of NW Europe the convective cloud lines are of more moderate intensity as in the example shown in Fig 30 - see the narrow curved line of cloud between XX in Fig 30(a). The cloud line at XX was one of three parallel cloud bands spaced 100km apart. Tracks of radar echoes associated with convective elements in one of these cloud bands (Fig 30(b)) show that, despite the modest depth (6km) and horizontal dimensions of individual convective cells, small clusters of such cells can retain their identity over many hours within a dry slot. However, this simplicity of behaviour tends to break down when, as over the Welsh hills on this occasion, additional convection is triggered by topography.

Rather similar convective bands have been studied by Bennetts and Ryder (1984) using closely spaced dropwindsondes. They found that conditional symmetric instability provided a plausible explanation of the mesoscale structure responsible for the bands. The tendency for the dry-slot convection to form in parallel lines may, alternatively, be due to forcing by pre-existing multiple vortex sheets (shear layers) within the dry-intrusion air, similar to those which were shown in Sec. 5 to be responsible for multiple bandedness in the vicinity of the

surface cold front. Similar interpretations may apply to the multiple bandedness and hyperfine baroclinic zones observed aloft in the main frontal cloud band by Kreitzberg (1968) and many others since.

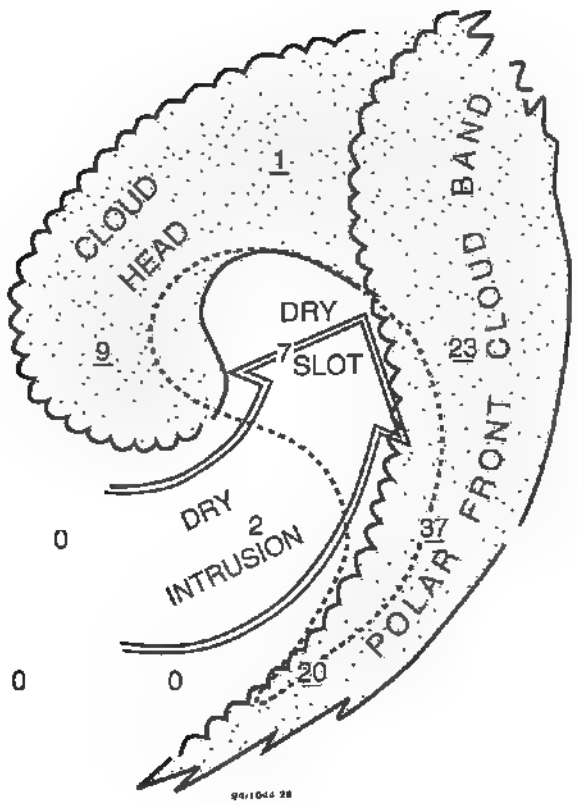


Fig.26 Occurrence of convection-related severe weather events in relation to the cloud pattern associated with a cyclone. The numbers represent percentage of events in the central USA occurring within subzones in the main cloud areas (underlined numbers) or developing within subzones of the dry slot (numbers not underlined) (from Carr and Millard 1985). Most of the underlined events occurred near the inner cloud boundary and so we have added the dashed line to show the main region of strong convection.

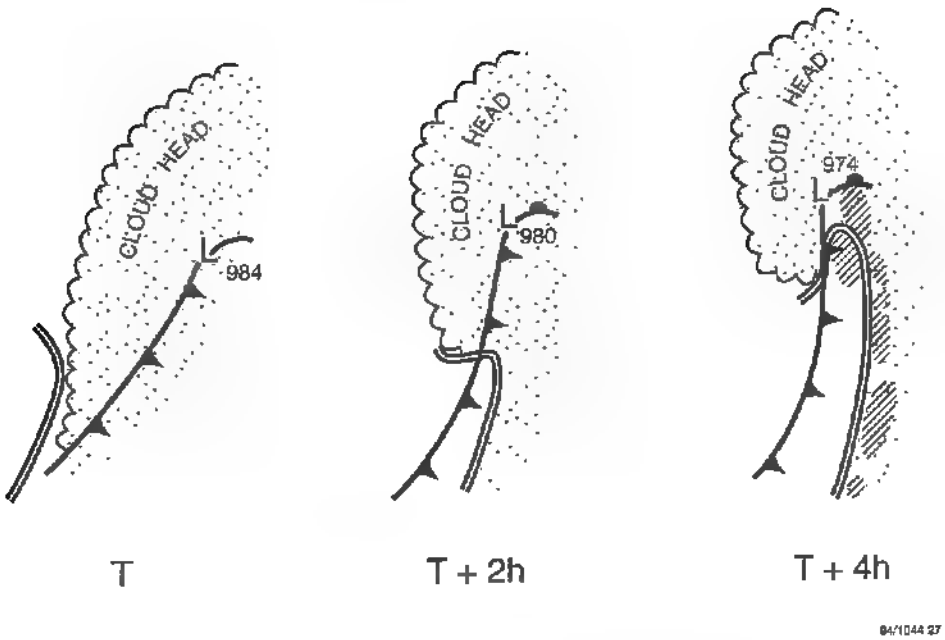


Fig.27 Simplified version of a diagram by Young et al (1987) showing the outbreak of deep convection within and along the leading edge of a dry slot at three consecutive times as the leading edge of a dry intrusion (double line) overran a surface cold front. Middle and upper-level cloud is shown stippled, part of which to the west of the cold front and cyclone centre (L) comprises the cloud head. Deep cumulonimbus which developed at T + 4h are shown hatched.

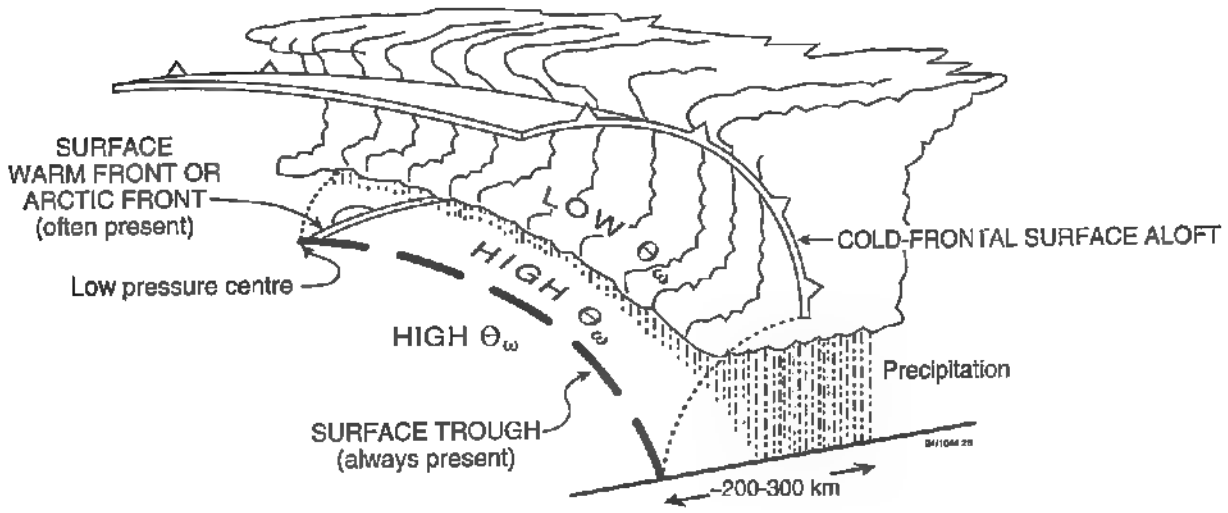


Fig.28 Schematic of a cold front aloft with a line of deep cumulonimbus situated ahead of a surface trough (Hobbs et al 1990).

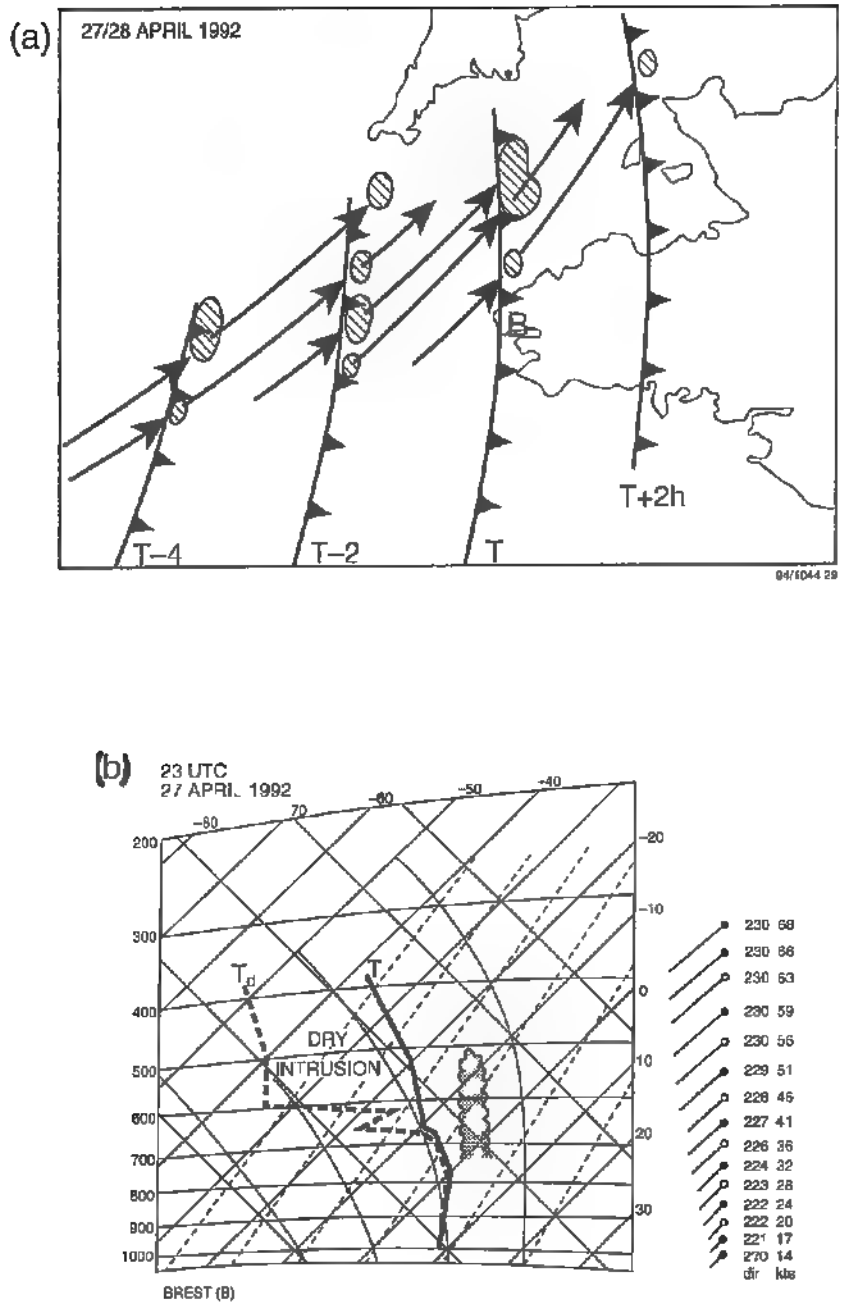


Fig.29 (a) Successive 2-hourly positions of an upper cold $\theta_w$-front showing the evolution of convective cells at its northern end near the cyclone centre. (b) Sounding from Brest (B) at the southern end of the line of cells at time T, showing the convective instability due to the overrunning dry intrusion and the vertical extent of the observed convection (Adapted from Browning et al 1995).

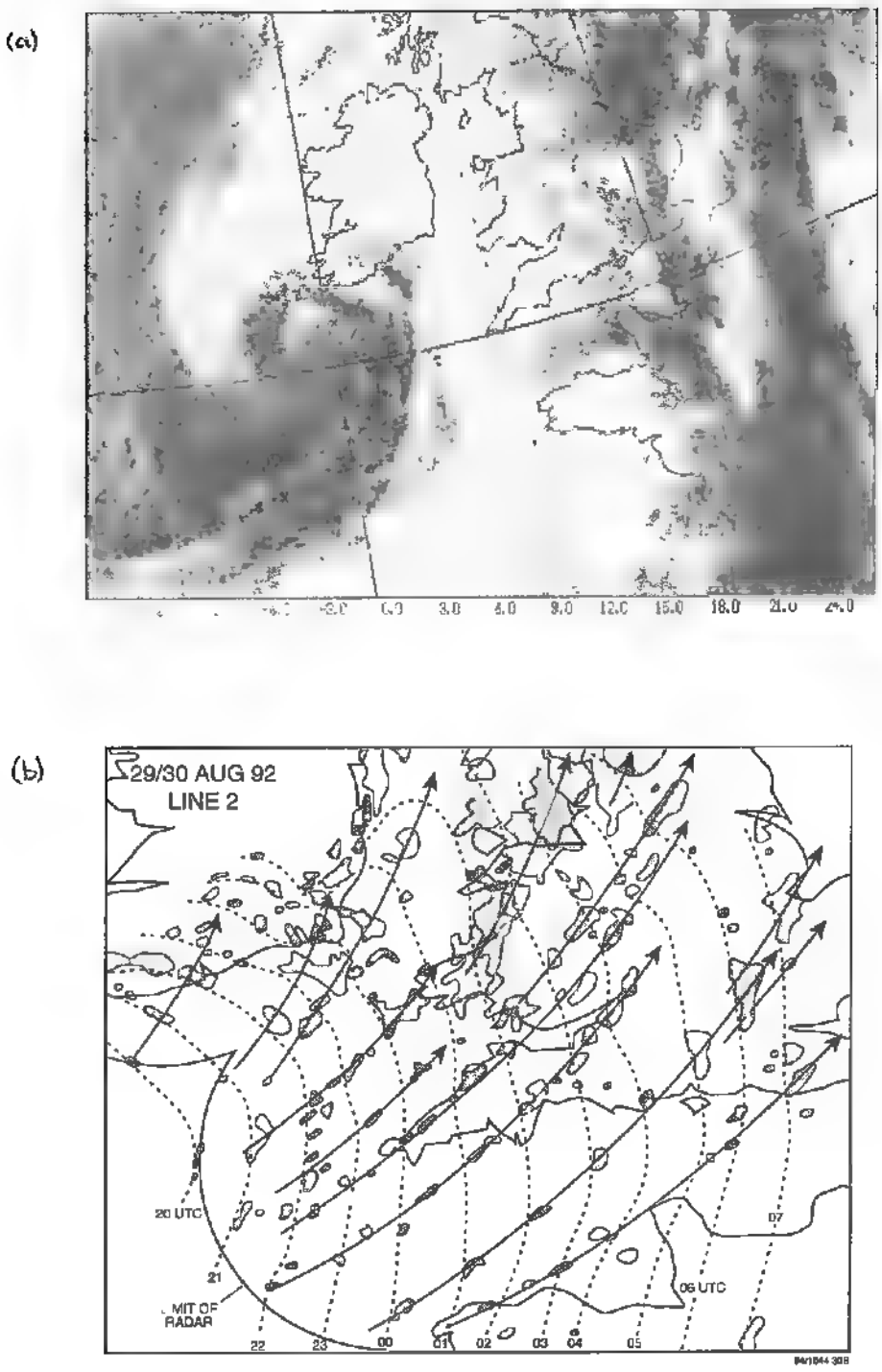


Fig.30 (a) Infra-red satellite image of a cyclone centred just off SW Ireland, showing convection within the dry slot. One of the three lines of convective cells that occurred in the dry slot can be seen between X and X. A brightness temperature scale is shown at the foot of the figure. (b) Hourly positions of one of the lines of convective cells as seen by radar as it crossed the British Isles within the dry slot. Areas with rain rate > 1 mm $h^{-1}$ are sketched and their tracks are indicated by arrows.

## 7. Concluding remarks

A theme that emerges from this review from an observational perspective is the major role played by the dry intrusion. The dry intrusion consists of air with low wet-bulb potential temperature ($\theta_w$) brought down from near tropopause level. Some of this air, originating just beneath the tropopause, has low potential vorticity (PV) and some of it, originating just above the tropopause, has high PV. The interesting mesoscale structures develop when the dry-intrusion air overruns a low-level baroclinic zone and air of increasingly high $\theta_w$ (ie a warm conveyor belt). The effect of the overrunning high PV is to trigger cyclogenesis and ascent. (The pockets of low PV air may lead to other forms of instability). The effect of the overrunning low-$\theta_w$ air is to develop potential instability which is realized by the ascent.

There is evidence of significant substructure within the dry-intrusion air. Small regions of locally higher PV in the dry intrusion organize the cloud and precipitation on the mesoscale and sometimes give rise to severe weather events. Progress in understanding these processes requires a combination of further observational, modelling and theoretical studies. There is currently a dearth of observations on the mesoscale, especially in the dry air where the only method of resolving the fine-scale structure is to release closely-spaced sondes, eg from high-flying aircraft. This will be one of the key objectives in the forthcoming Fronts and Atlantic Storm Track Experiment (FASTEX).

The importance of upper-level PV anomalies for cyclogenesis is already well established: what is still a matter of debate is the extent to which the upper-level factors dominate the evolution of the weather systems. If they are confirmed in having a dominant

role this will point to the operational need for improved upper-level observations, particularly of the winds near tropopause level. There is evidence (eg Browning and Reynolds 1994, Browning and Golding 1995) that mesoscale events, including severe wind and precipitation events associated with convection, are closely related to the descent of mesoscale PV maxima within dry intrusions. If further research shows that this association has some generality, it will signify an opportunity for improving short period forecasts of severe weather. To realize such an opportunity, additional observations would be needed in an era when all the pressures are towards reducing such costs. However, if we are correct in suspecting that it is wind observations at a particular level that are most required, then it may be possible eventually to develop a focussed strategy for meeting the requirement.

**Acknowledgements**

I am grateful to Mike Bader, Sid Clough, Roger Grant, Tim Hewson and Martin Young for helpful comments on an earlier draft.

## References


Bader, M.J., G.S. Forbes, J.R. Grant, R.B.E. Lilley, and A.J.Waters (Eds.) 1994: Images in weather forecasting. Cambridge University Press. In press.

Bennetts, D.A. and P. Ryder, 1984: A study of mesoscale convective bands behind cold fronts. Part 1: Mesoscale organization, *Quart.J.Roy.Meteor.Soc.*, 110, 121-145.

Bergeron, T., 1937: On the physics of fronts. *Bull.Amer.Meteor.Soc.*, 18, 265-275.

Böttger, H., M. Eckardt, and U. Katergiannakis, 1975: Forecasting extratropical storms with hurricane intensity using satellite information. *J.Appl.Meteor.*, 14, 1259-1265.

Browning, K.A., 1990: Organization of clouds and precipitation in extratropical cyclones. In 'Extratropical cyclones. The Erik Palmén Memorial Volume'. *Amer.Meteor.Soc.*, pp 129-153.

Browning, K.A., 1994: Life cycle of a frontal cyclone. *Met.Apps.*, 1, ~~XXX-XXX~~. 233-235

Browning, K.A., 1995: On the nature of the mesoscale circulations at a kata-cold front. *Tellus A*.

Browning, K.A., S.A.,Clough, C.S.A. Davitt, N.M. Roberts, T.D. Hewson and P.G.W. Healey, 1995: Observations of the mesoscale sub-structure in the cold air of a developing frontal cyclone, *Quart.J.Roy.Meteor.Soc.*, 121, XXX-XXX.

Browning, K.A. and B.W. Golding, 1995: Mesoscale aspects of a dry intrusion within a vigorous cyclone. *Quart.J.Roy.Meteor.Soc.*, 121, XXX-XXX.

Browning, K.A., and F.F. Hill, 1985: Mesoscale analysis of a polar trough intersecting with a polar front. *Quart.J.Roy.Meteor.Soc.*, 111, 445-462.

Browning, K.A. and G.A. Monk, 1982: A simple model for the synoptic analysis of cold fronts. *Quart.J.Roy.Meteor.Soc.*, 108, 435-452.

Browning, K.A. and R. Reynolds, 1994: Diagnostic study of a narrow cold-frontal rainband and severe winds associated with a stratospheric intrusion. *Q.J.R.Meteor.Soc.*, 120, 235-257.

Browning, K.A. and N.M. Roberts, 1994: Structure of a frontal cyclone. *Quart.J.Roy.Meteor.Soc.*, 120, 1535-1557.

Carbone, R.E., 1982: A severe frontal rainband. Part 1: Stormwide hydrodynamic structure. *J.Atmos.Sci.*, 39, 258-279.

Carlson, T.N., 1980: Airflow through midlatitude cyclones and the comma cloud pattern. *Mon.Wea.Rev.*, 108, 1498-1509.

Carr, F.H. and J.P. Millard, 1985: A composite study of comma clouds and their association with severe weather over the Great Plains, *Mon.Wea.Rev.*, 113, 370-387.

Danielsen, E.F., 1964: Project Springfield Report. Defense Atomic Support Agency, Washington D.C. 20301, DASA 1517 (NTIS # AD-607980), 97 pp.

Evans, S.M., D. Keyser, Bosart and G.M. Lackmann, 1994: A satellite-derived classification scheme for L.F. rapid maritime cyclogenesis *Mon.Wea.Rev.*, 122, 1381-1416.

Harrold, T.W., 1973: Mechanisms influencing the distribution of precipitation within baroclinic disturbances. *Quart.J.Roy.Meteor.Soc.*, 99, 232-251.

Hobbs, P.V., J.D. Locatelli and J.E. Martin, 1990: Cold fronts aloft and the forecasting of precipitation and severe weather east of the Rocky Mountains. *Wea.Forecasting*, 5, 613-626.

Hobbs, P.V. and P.O.G. Persson, 1982: The mesoscale and microscale structure and organization of clouds and precipitation in midlatitude cyclones. Part V: The substructure of narrow cold-frontal rainbands. *J.Atmos.Sci.*, 39, 280-295.

Hoskins, B.J., M.E. McIntyre, A.W. Robertson, 1985: On the use and significance of isentropic potential vorticity maps. *Quart.J.Roy.Meteor.Soc.*, 111, 877-946.

Kreitzberg, C.W., 1968: The mesoscale wind field in an occlusion. *J.Appl.Meteor.*, 7, 53-67.

Kuo, Y-H., R.J. Reed and S. Low-Nam, 1992: Thermal structure and airflow in a model simulation of an occluded marine cyclone, *Mon.Wea.Rev.*, 120, 2280-2297.

Letestu, A.-C., 1994: Case study analysis of warm conveyor belt and low level jet phenomena. PhD Thesis, Univ.of.Reading, 210 pp.

McGinnigle, J.B., M.V. Young, and M.J. Bader, 1988: The development of instant occlusions in the North Atlantic. *Meteor.Mag.*, 117, 325-341.

Mansfield, D. 1994: The use of potential vorticity in forecasting cyclones: operational aspects. In 'The life cycles of extratropical cyclones, Vol III', proc. international symposium, 27 June-1 July 1994, Bergen, pp 326-331.

Mass, C.F. and D.M. Schultz, 1993: The structure and evolution of a simulated midlatitude cyclone over land. *Mon.Wea.Rev.*, 121, 889-917.

Monk, G.A. and M.J. Bader, 1988: Satellite images showing the development of the storm of 15-16 October 1987, *Weather*, 43, 130-135.

Reed, R.J., 1955: A study of a characteristic type of upper level frontogenesis. *J.Meteor.*, 12, 226-237.

Rodgers, D.M., M.J. Magnano J.H. Arns, 1985: Mesoscale convective complexes over the US and during 1983. *Mon. Wea.Rev.*, 113, 888-901.

Shapiro, M.A. and D. Keyser, 1990: Fronts, jet streams and the tropopause. In 'Extratropical cyclones. The Erik Palmén Memorial Volume', *Amer.Meteor.Soc.*, pp 167-191.

Shutts, G.J., 1990: Dynamical aspects of the October storm, 1987: A study of a successful fine-mesh simulation. *Quart.J.Roy.Meteor.Soc.*, 116, 1315-1347.

Uccellini, L.W., D. Keyser, K.F. Brill and C.H. Wash, 1985: The Presidents' Day cyclone of 18-19 February 1979: Influence of upstream trough amplification and associated tropopause folding on rapid cyclogenesis. *Mon.Wea.Rev.*, 113, 962-988.

Weldon, R.B., 1977: An oceanic cyclogenesis - its cloud pattern and interpretation. NWS/NESS Satellite Applications Information Note 77/7, 11 pp.

Wernli, H. and A.M. Rossa, 1994: Identification of structures within extratropical cyclones based upon objective criteria. In 'The life cycles of extratropical cyclones, Vol II', proc. international symposium, 27 June-1 July 1994, Bergen, pp 548-553.

Young, M.V., 1989: Investigation of a cyclogenesis event, 26-29 July 1988, using satellite imagery and numerical model diagnostics. *Meteor.Mag.*, 118, 185-196.

Young, M.V., 1994: A classification scheme for cyclone life-cycles: applications in analysis and short-period forecasting. In 'The life cycles of extratropical cyclones, Vol III', proc international symposium, 27 June-1 July 1994, Bergen. pp 380-385.

Young, M.V., G.A. Monk and K.A. Browning, 1987: Interpretation of satellite imagery of a rapidly deepening cyclone. *Quart.J.Roy.Meteor.Soc.*, 113, 1089-1115.

Zillman, J.W., and P.G. Price, 1972: On the thermal structure of mature Southern Ocean cyclones. *Austral.Meteor.Mag.*, 20, 34-48.

## CURRENT JCMM INTERNAL REPORTS

This series of JCMM Internal Reports, initiated in 1993, contains unpublished reports and also versions of articles submitted for publication. The complete set of Internal Reports is available from the National Meteorological Library on loan, if required.

1. **Research Strategy and Programme**
   K A Browning et al
   January 1993

2. **The GEWEX Cloud System Study (GCSS)**
   **GEWEX Cloud System Science Team**
   January 1993

3. **Evolution of a mesoscale upper tropospheric vorticity maximum and comma cloud from a cloud-free two dimensional potential vorticity anomaly**
   K A Browning
   January 1993

4. **The Global Energy and Water Cycle**
   K A Browning
   July 1993

5. **Structure of a midlatitude cyclone before occlusion**
   K A Browning and N Roberts
   July 1993

6. **Development in Systems and Tools for Weather Forecasting**
   K A Browning and G Szejwach
   July 1993

7. **Diagnostic study of a narrow cold frontal rainband and severe winds associated with a stratospheric intrusion**
   K A Browning and R Reynolds
   August 1993

8. **Survey of perceived priority issues in the parametrizations of cloud-related processes in GCMs**
   K A Browning
   September 1993

9. **The Effect of Rain on Longwave Radiation**
   I Dharssi
   September 1993

10. **Physical Cloud Microprocesses - A Description of the Parametrization used in the Large Eddy Model**
    H Swann
    July 1994

11. **An Appreciation of the Meteorological Research of Ernst Kleinschmidt**
A J Thorpe
May 1992

12. **Potential Vorticity of Flow Along the Alps**
A J Thorpe, H Volkert and Dietrich Heimann
August 1992

13. **The Representation of Fronts**
A J Thorpe
January 1993

14. **A Parametrization Scheme for Symmetric Instability: Test for an Idealised Flow**
C S Chan and A J Thorpe
February 1993

15. **The Fronts 92 Experiment: a Quicklook Atlas**
Edited by T D Hewson
November 1993

16. **Frontal wave stability during moist deformation frontogenesis**
**Part 1. Linear wave dynamics**
C H Bishop and A J Thorpe
May 1993

17. **Frontal wave stability during moist deformation frontogenesis**
**Part 2. The suppression of non-linear wave development**
C H Bishop and A J Thorpe
May 1993

18. **Gravity waves in sheared ducts**
C Bishop and A J Thorpe
November 1993

19. **Potential Vorticity and the Electrostatics Analogy: Quasi-Geostrophic Theory**
C Bishop and A J Thorpe
November 1993

20. **Recent Advances in the Measurement of Precipitation by Radar**
A J Illingworth
April 1993

21. **Micro-Physique et Givrage. Cloud Microphysics and Aircraft Icing**
A J Illingworth
May 1993

22. **Differential Phase Measurements of Precipitation**
M Blackman and A J Illingworth
May 1993

23. **Estimation of Effective Radius of Cloud Particles from the Radar Reflectivity**
N I Fox and A J Illingworth
May 1993

24. **A Simple Method of Dopplerising a Pulsed Magnetron Radar**
A Hau, A J Illingworth and J Eastment
November 1993

25. **Radiation and Polar Lows**
George C Craig
February 1994

26. **Collected preprints submitted to the International Symposium on the Life Cycles of Extratropical Cyclones; Bergen, Norway, 27 June - 1 July 1994**
April 1994

27. **Convective Frontogenesis**
Douglas J Parker and Alan J Thorpe
April 1994

28. **Improved Measurement of the Ice Water Content in Cirrus Using a Total Water Evaporator**
Philip R A Brown and Peter N Francis
April 1994

29. **Mesoscale Effects of a Dry Intrusion within a Vigorous Cyclone**
K A Browning and B W Golding
April 1994

30. **GEWEX Cloud System Study, Science Plan**
May 1994

31. **Parametrization of Momentum Transport by Convectively Generated Gravity Waves**
R Kershaw
February 1995

32. **Mesoscale Modelling Newsletter No 5**
May 1994

33. **Observations of the mesoscale sub-structure in the cold air of a developing frontal cyclone**
K A Browning, S A Clough, C S A Davitt, N M Roberts and T D Hewson
May 1994

34. **Longwave Radiative Forcing of a Simulated Tropical Squall Line**
Imtiaz Dharssi
July 1994

35. **On the nature of the convective circulation at a kata-cold front**
K A Browning
September 1994

36. **Collective preprints of papers submitted to the COST-75 International Seminar on Advanced Weather Radar Systems, Brussels, 20-23 September 1994**
November 1994

37. **Use of satellite imagery to diagnose events leading to frontal thunderstorms: Parts 1 and 11 of a case study**
K A Browning and N M Roberts
November 1994

38. **The role of spaceborne millimetre-wave radar in the global monitoring of ice cloud**
P R A Brown, A J Illingworth, A J Heymsfield, G M McFarquahar, K A Browning and M Gosset
December 1994

39. **Potential Vorticity Inversion**
Michael Ziemianski
October 1994

40. **Theory of mature tropical cyclones; a comparison between Kleinschmidt (1951) and Emanuel (1986)**
Suzanne L Gray
December 1994

41. **Dispersion and removal of pollutants during the passage of an atmospheric frontal system**
N R Gimson
December 1994

42. **The role of snow sublimation in frontogenesis**
D J Parker and A J Thorpe
December 1994

43. **Potential vorticity and the electrostatics Analogy: Ertel-Rossby formulation**
A J Thorpe and C H Bishop
December 1994

44. **Mesoscale aspect of extratropical cyclones: an observational perspective**
K A Browning
January 1995

**Met Office** Joint Centre for Mesoscale Meteorology Department of Meteorology
University of Reading PO Box 243 Reading RG6 6BB United Kingdom
Tel: +44 (0)118 931 8425 Fax: +44 (0)118 931 8791
www.metoffice.com